Corrosion behaviour of low temperature nitrided nickel-free, AISI 200 and AISI 300 series austenitic stainless steels in NaCl solution

(Article begins on next page)

09 January 2025

Corrosion behaviour of low temperature nitrided nickel-free, AISI 200 and AISI 300 series austenitic stainless steels in NaCl solution

Francesca Borgioli*, Emanuele Galvanetto, Tiberio Bacci

Department of Industrial Engineering (DIEF), University of Florence, via S. Marta 3, 50139 Florence, Italy

* Corresponding author:

Department of Industrial Engineering (DIEF)

University of Florence

via S. Marta 3

50139 Florence

Italy

Phone: + 39 055 2758 734

Fax: + 39 055 2758 755

e-mail: francesca.borgioli@unifi.it

Highlights

- Alloy composition influences the corrosion resistance of nitrided stainless steels

- S phase without nitrides can be obtained on nickel-free austenitic stainless steel

- Nitrogen surface alloying increases nobility of austenitic stainless steels

- Tendency to resist localized corrosion phenomena is AISI 202 < AISI 316L < P558

Abstract

Low temperature plasma nitriding was performed on CrNi-based (AISI 316L), CrMn-based (AISI

202) and nickel-free (P558) austenitic stainless steels. For all the used steels modified surface layers consist mainly of S phase without the precipitation of large amounts of nitrides, and they show enhanced surface microhardness and corrosion resistance in NaCl acqueous solution. The different electrochemical corrosion testing techniques evidence that the increase of corrosion potential may be ascribed mainly to nitrogen addition, while regarding the increase of potential, at which localized corrosion phenomena occur, also alloy elements, and in particular Mo, play an important role.

1. Introduction

Nitrogen addition in austenitic stainless steels is considered an important tool for improving tensile properties [1-3] and localized corrosion resistance [1,4,5] of these alloys. As alloy element, nitrogen is present not only as fairly small addition in traditional steels, as in AISI 316LN (about $0.1 - 0.16$ wt.%), but it is added in larger amounts in the "high-nitrogen" stainless steels (> 0.4 wt.%, according to Speidel [6]) and in the so called nickel-free stainless steels, in which it is used together with manganese as an austenite stabilizing element instead of nickel [1].

The effect of nitrogen on general corrosion of austenitic stainless steels is still a matter of debate, since both positive [3,7] and negative [8,9] effects have been reported, while there is an accordance on its beneficial effects when localized corrosion phenomena may occur [1,4,5,10]. Nitrogen is able to promote passivity, widen the passive range, enhance stress corrosion cracking resistance in some media and improve the resistance to intergranular corrosion [1,4-6,10]. Many theories have been proposed on the protection mechanisms of nitrogen. The main ones are as follows.

(1) N atoms, released during the early stages of the corrosion process, may react with H^+ forming ammonium ions (NH_4^+), which locally increase the pH in incipient pits or crevices and promote repassivation [4,10-12]. It has also been proposed that NH_4^+ ions could form corrosion inhibiting nitrates [12], they may react with free chlorine in chlorinated waters, forming less oxidizing species [13], and they may produce a protective passive ammonium sulphate layer in sulphate solutions [14].

(2) N enrichment at the film/substrate interface may occur during passivation, so anion attack is prevented [11,15]. An incorporation of N and ammonium ions in the passive film has also been observed [15].

(3) An accumulation of negatively charged nitrogen at the passive layer might have a repulsive action towards Cl^-, so that a faster repassivation may be promoted [16,17].

Surface alloying with nitrogen can be obtained on austenitic stainless steels by means of low temperature nitriding [1,18]. When treatments are performed at temperatures lower than 450 °C, the

precipitation of large amounts of chromium nitrides does not usually occur, so that the decrease of corrosion resistance due to chromium depletion from solid solution is avoided [19]. At these nitriding temperatures a supersaturated solid solution of nitrogen in the expanded and distorted austenite lattice is able to form [1,18,19]. This phase, known as S phase [1,18-20] or expanded austenite [1,21], has a nitrogen content up to about 10 wt.% [18], a high hardness (up to about 1500 HV [18]) and a high corrosion resistance in chloride-ion containing solutions [18-20]. It has been hypothesized that the increase of corrosion resistance observed for nitrided samples, in comparison with untreated ones, is due to mechanisms similar to those observed for N-containing austenitic stainless steels [18,22,23].

The effect of low temperature nitriding on corrosion behaviour has been studied especially for AISI 300 series stainless steels [18,20,22-29]; a few researches have been also performed on AISI 200 series stainless steels [20,29,30]. Very few studies have regarded nickel-free austenitic stainless steels [31,32]. Nitriding of these steels was observed to produce large amounts of nitrides, which decrease the corrosion resistance, so it was concluded that is difficult to obtain a modified layer consisting of S phase with a pure nitriding treatment [18,31,32]. Little attention has been paid on the direct comparison of the effects of nitriding on austenitic stainless steels of different types [24-26,28,29] or different series [29,33].

In the present research a direct comparison of the effects of low temperature nitriding on the characteristics of the modified layers produced on CrNi-based AISI 300 series (AISI 316L), CrMn-based AISI 200 series (AISI 202) and nickel-free (P558) austenitic stainless steels was carried out. The microstructure, phase composition and surface microhardness of the nitrided steels were investigated. Corrosion behaviour of the nitrided samples in NaCl aqueous solution was studied by means of electrochemical impedance spectroscopy (EIS) analysis, open circuit potential (OCP) measurements, potentiodynamic and galvanostatic tests, and the results were compared also with those of the untreated alloys.

2. Experimental procedure

Three austenitic stainless steels were employed, AISI 316L and AISI 202, supplied by ThyssenKrupp Acciai Speciali Terni (Italy), and the nickel-free P558, supplied by Böhler Uddeholm Italia S.p.a. (Italy); the chemical composition of the alloys is reported in Table 1. Taking into account the chemical composition, the Pitting Resistance Equivalent Number (PREN) of the alloys was 24.0 for AISI 316L, 19.4 for AISI 202, and 36.1 for P558. AISI 316L and AISI 202 steels were in the form of cold rolled, annealed and pickled plates, which were cut for obtaining prismatic samples (39 x 16 x 0.7 mm). P558 was in the form of a rod (diameter: 18 mm), and it was cut in order to obtain disks (diameter: 18 mm; thickness: 0.7 mm). All the samples were ground with SiC papers and polished up to 6-μm diamond suspension.

Low temperature glow-discharge nitriding treatments were performed in a laboratory plasma equipment using a d.c. power supply. The samples were put on a horizontal sample holder placed in the centre of the treatment chamber. The sample holder was connected to the cathode of the power supply and it was surrounded by an AISI 304 screen, which was grounded and worked as anode. The anode-cathode distance was about 70 mm. The treatment temperature was controlled varying the discharge current supplied by the d.c. power supply and it was measured by a chromel-alumel thermocouple inserted into the sample holder. At first, after evacuating the treatment chamber up to a pressure of about 5 Pa, a cathodic sputtering was carried out for removing the natural passive film and enabling a homogeneous nitriding process; the ion bombardment allowed also the heating of the samples. The sputtering was performed at 110 Pa with a gas composition of 80 vol. % N_2 and 20 vol. % H_2 using a constant current density of 1.50 ± 0.01 mA cm^{-2}, until a temperature of 300 °C was reached. Then temperature, pressure and treatment atmosphere were changed to their nominal values. Nitriding treatments were performed at 360 and 380 °C, at a constant pressure of 340 Pa, for 3 h, using a gas mixture of 50 vol. % N_2 and 50 % vol. H_2 in a 400 sccm total flow rate. The current density and voltage drop depended on nitriding temperature, and they were 1.09 ± 0.05 mA cm^{-2} and 185 ± 5 V for the 360-°C treatment, and 1.19 ± 0.05 mA cm^{-2} and 198 ± 5 V for the 380-°C

treatment.

The microstructure of the untreated and nitrided samples was examined using light and scanning electron (SEM) microscopies and energy dispersion spectroscopy (EDS) analysis. Cross-sections were obtained by cutting the samples and mounting them with glass-filled epoxy thermosetting resin. Taper sections with a 10°-angle were obtained for selected samples by cold mounting them in epoxy resin. The microstructure of the modified layers and of the matrix was delineated using acetic glyceregia etchant (3 ml HCl, 2 ml HNO_3, 2 ml acetic acid, 1 drop of glycerol).

A semi-quantitative evaluation of the alloy elements (Fe, Cr, Ni, Mo, Mn, Si) and of nitrogen present in the surface layers of the samples was performed by means of X-ray fluorescence (XRF) analysis.

The phases present in the surface layers were identified by means of X-ray diffraction analysis (Cu Kα radiation). Diffraction patterns were collected in Bragg-Brentano configuration and with a 10°-constant incident angle; in this latter configuration, the mean penetration depth (i.e., the depth at which the intensity drops by a factor of e) is 0.6 μm.

Roughness measurements were carried out by means of a stylus profilometer tester, using a 2-μm radius stylus with a 1-mN contact force; the cut-off length was 0.25 mm. Ten measurements were taken at different locations on each sample. The average surface roughness Ra (arithmetical mean deviation of the roughness profile from the mean line), the maximum height of profile Rz (sum of the largest profile peak height and the largest profile valley depth within a sampling length, according to EN ISO 4287-2009 norm) and the mean height of profile elements Rc (mean value of the profile element heights within a sampling length) were recorded.

Surface microhardness measurements (load: 25, 50 and 100 gf) were carried out on the surface of the samples using a Knoop indenter.

Corrosion resistance of untreated and nitrided samples was studied in a 5 % NaCl solution at room temperature in naturally aerated conditions without stirring. The solution was prepared with distilled water and analytical grade chemicals. A three-electrode electrochemical flat cell equipped

with an Ag/AgCl reference electrode (3.5 M KCl) and a platinum grid as counterelectrode was used. All the potential values in the paper are given versus the reference electrode. The sample surface area exposed to the electrolyte was 1 cm^2. At least three electrochemical tests for each sample type were carried out for assessing the result.

All the electrochemical tests were performed after 18-h delay; during the delay the open circuit potential (OCP) was recorded.

Electrochemical impedance spectroscopy (EIS) measurements were carried out at OCP. The frequency range was between 10 kHz to 12 mHz, with 10 points per decade and an *ac* amplitude (rms) of 5 mV. EIS spectra were modelled using a non linear least square analysis software (EIS Spectrum Analyser [34]).

Potentiodynamic polarization tests were carried out at a rate of 0.3 mV s^{-1}. The degradation due to corrosion phenomena was evaluated further by means of a coulometric analysis. The anodic polarization curves were arbitrarily divided into three distinct zones: the first zone (zone I) ranged from corrosion potential to + 500 mV, the second zone (zone II) from + 500 to + 1000 mV, and the third one (zone III) from + 1000 to + 1200 mV. Current density values of the polarization curves were integrated for each zone, taking into account that

potential (mV) / scan rate (mV s^{-1}) = time (s)

The integration was performed using the program Echem Analyst (Gamry). The results were expressed as charge density (mC cm^{-2}).

The samples were characterized further using the galvanostatic method. It consists in imposing a constant anodic current to the working electrode and recording the corresponding potential as a function of time. In this way the amount of electrochemically inflicted damage can be controlled. This technique has been used to characterize the corrosion behaviour of many alloys when pitting [35-37] or crevice [38,39] phenomena occur.

In the chronopotentiometric curves three distinct regions are usually observed [35,38].

In the first one (Region I), usually short living, potential value increases with time, and a

galvanostatic growth of the passive layer occurs. The potential value reaches a maximum (E_{max}), which corresponds to the beginning of the surface activation, with the pit [35] or crevice [38] nucleation. This maximum value has been regarded as the pitting potential, when only pitting is present [35].

The second region (Region II) corresponds to the pitting or crevice propagation stage. This region may show potential fluctuations due to transient passive film repair/breakdown.

The third region (Region III), in which a stationary potential value tends to be reached (E_{min}), has been ascribed to either repassivation phenomena [35] or stable pit or crevice growth [37,38]. Despite the different nature of these phenomena, the stationary potential can be regarded as the minimum potential, below which pitting or crevice phenomena do not develop [40].

Galvanostatic tests were performed imposing a constant anodic current of 100 $\mu A\ cm^{-2}$ and the potential variation was recorded for 1 h.

3. Results

3.1 Morphology and microstructure

The untreated samples have a fairly smooth surface, with shallow grooves due to grinding and polishing. X-ray diffraction analysis shows that, besides austenite, γ-Fe (f.c.c.), a very small amount of ferrite, α-Fe (b.c.c.) is present in all the steels; the peaks of α-Fe overlap those of b.c.t. α' martensite, which may also form during grinding and polishing. In P558 samples a small amount of ε' martensite (h.c.p.) was also observed, probably due to the grinding and polishing procedure.

When nitriding is performed, the surface of all the samples shows characteristic features, previously described [20,41]. Plasma etching, due to both sputtering and nitriding treatments, delineates the austenitic microstructure with the characteristic twins. The grooves due to the grinding and polishing procedure are still observable. When the samples are nitrided at 360 °C, etching is fairly light (Fig. 1 a, b, c), but it causes a significant roughness increase in comparison with untreated samples (Table 2). Cross-section examination of the nitrided samples shows that the modified

8

surface layers have a double layer microstructure (Fig. 2 a, b, c). The chemical etching delineates homogeneous layers, which are separated one from the other by etched lines. The thickness of the modified layers is reported in Table 3. In the outer layer of AISI 316L and AISI 202 samples groups of shear lines, which extend from the outer surface into the layer itself, are present (Fig. 2 a, b). As previously reported [29], these lines are fewer and extend less deeply in AISI 316L samples in comparison with AISI 202 ones. In P558 samples very few and short shear lines are observable (Fig. 2 c). According to X-ray diffraction analysis, the outer modified layer consists of S-phase (Fig. 3). The peaks of a solid solution of nitrogen in h.c.p. martensite, ε_N', are also present. This phase is considered analogous to the strain induced h.c.p. martensite, but with larger lattice parameters due to nitrogen solubilization [42]. The inner modified layer is homogeneous for all the treated steels and it consists of a solid solution of interstitial atoms (nitrogen, carbon) in the slightly expanded austenite lattice, γ(N,C), as also previously observed [29]. According to EDS analysis, the S phase, γ(N,C) and the matrix have a comparable composition of alloy elements Cr, Ni, Mn, Mo, as previously reported [29]. XRF analysis shows that in the surface layers nitrogen content significantly increases, in comparison with the untreated samples (Table 1): in AISI 316L and AISI 202 samples N content is about 22 at.%, while in P558 ones is about 19 at.%.

When nitriding is carried out at 380 °C, the surface of the samples is etched more strongly and additional features are observable: reliefs are present at grain boundaries and some grain boundaries lean forward on adjacent grains. On all sample types shear bands are well delineated within the grains (Fig. 4 a, b, c). The presence of local plastic deformations occurring during the formation of the modified layers was previously reported [18,20,29,43]. These additional features cause a further roughness increase, which is greater for AISI 316L and AISI 202 samples than for P558 ones (Table 2), in accordance with microscopy observations. The modified surface layers still show the characteristic double layer microstructure (Fig. 5 a, b, c). The shear lines are well observable in all the samples and they extend more deeply in the outer layer of AISI 202 and P558 samples than in that of AISI 316L ones. The thickness of the modified layers is significantly higher than that of 360-

°C nitrided samples (Table 3). X-ray diffraction analysis shows that the peaks of S phase shift towards lower angles, so that a further lattice expansion due to a higher nitrogen solubilization may be supposed (Fig. 6). Besides S phase, also ε_N' was detected. The presence of h.c.p. ε-type nitride, $M_{2-3}N$ (M=Fe, Cr, Mn, Mo, Ni), which may form as a consequence of a distortion of ε_N' martensite and an ordering of nitrogen atoms [44], cannot be completely ruled out, even if distinct peaks of this phase were not observed. The formation of ε-nitride for AISI 316L and AISI 202 usually occurs at higher nitriding temperatures [20,29], so the presence of this phase may not be plausible for these steels. On the other hand, the high manganese content of P558 steel may promote the formation of ε-nitride; on account of this hypothesis, for the pattern of the 380-°C nitrided sample the symbol of this phase is shown in parentheses (Fig. 6 c). However, strongly etched regions, which are usually related to nitrides [29], were not observed in all the studied samples either cross- or taper sectioned. XRF analysis shows that in the surface layers nitrogen content increases in comparison with the samples nitrided at 360 °C, and it reaches about 25 at.% in AISI 316L and AISI 202, while in P558 is about 29 at.%.

3.2 Surface microhardness

Surface microhardness values of untreated and nitrided samples are depicted in Fig. 7. For all the considered steels the surface microhardness of the nitrided samples is greater than that of the untreated ones, and it increases as the treatment temperature is higher. As the load is increased, lower hardness values are detected, due to both the indentation size effect and the fact that layers having different characteristics are tested.

Using 50 and 100 gf loads, nitrided P558 samples have greater microhadness values in comparison with the other sample types, due to the higher hardness of the matrix substrate.

3.3 Corrosion behaviour

3.3.1 Open Circuit Potential Curves

Typical Open Circuit Potential (OCP) curves, recorded as a function of time, for untreated and nitrided samples are shown in Fig. 8.

The OCP curves for all the untreated samples have similar features, with a decrease of the potential values down to a minimum and then a slow increase. This potential decrease, as also reported by other authors [45], may be ascribed to a degradation of the air-formed passive layer due to the adsorption of Cl$^-$ ions [46,47]. The potential decrease due to the action of chlorides is faster for AISI 202 (Fig. 8 b), while it is slower for P558 (Fig. 8 c), but after a lapse of time the potential stops to decrease and a shift towards more positive values is observed, suggesting that repassivation phenomena occur. The superposition of fairly sharp decreases and increases of potential values may be ascribed to pit nucleation and repassivation phenomena.

On the other hand, the nitrided samples show a potential increase trend with fluctuations due to metastable pit formation and repassivation. The pit repassivation kinetics is slower in comparison with that of the untreated samples, as previously observed [48].

At the end of the delay time all the nitrided samples have higher potential values than those of untreated ones, suggesting a more noble behaviour.

3.3.2 Electrochemical Impedance Spectroscopy analysis

The typical EIS spectra of untreated and nitrided samples tested at the respective OCP are shown in Fig. 9 in the form of Bode (a, c, e) and Nyquist (b, d, f) plots.

In order to obtain a physical picture of the corrosion behaviour of the system the experimental data were modelled using appropriate electrical equivalent circuits (EEC), represented in Fig. 10; the EEC parameter values obtained by fitting experimental data are reported in Tables 4 and 5.

The analysis of phase angle plots of untreated samples shows the presence of an asymmetry, which becomes a clear second inflection of the curve for all the nitrided samples except for 380-°C nitrided P558. This feature suggests the presence of two time constants which are partially overlapped. A similar EEC is usually used for modelling data of austenitic stainless steels put in

11

contact with many solutions [49-51]. The high frequency (HF) time constant may be related to the faster charging/discharging processes occurring at the electrode/electrolyte interface, while the low frequency (LF) time constant to the slower processes occurring in the oxide phase. In this EEC model, depicted in Fig. 10 a, the electronic elements have the following meanings: R_s is the electrolyte resistance, for the HF time constant R_{ct} is the charge transfer resistance and CPE_{dl} represents the double layer/space charge capacitance, for the LF time constant R_o and CPE_o take into account charge transfer and mass transport processes occurring in the oxide phase. The sum of R_{ct} and R_o, R_{tot}, can be considered a measure of the surface total resistance to general corrosion [50]. A better fitting is obtained if constant phase elements (CPE) are used instead of pure capacitances. The use of CPE is due to a distribution of relaxation times as a result of inhomogeneities as surface roughness/porosity, adsorption and diffusion [49,52,53]. The impedance of CPE is defined as:

$Z = [CPE\ (i\omega)^n]^{-1}$

where CPE is a constant parameter, ω is the angular frequency, $i^2 = -1$ is the imaginary number and n is the CPE exponent. Depending on n, CPE can represent a pure capacitance ($n = 1$), a pure resistance ($n = 0$), a pure inductance ($n = -1$), or a Warburg impedance, i.e. a mass transport related impedance ($n = 0.5$). The deviation of n from these values indicates a deviation from the ideal behaviour of the system. This deviation from an ideal capacitive behaviour is observed for all the samples. For the HF time constant, the CPE exponent, n_{dl}, is very close to unity for all the tested samples. The deviation from a pure capacitance behaviour of the double layer may be ascribed to surface heterogeneities at the micrometric (roughness, polycrystalline structure) and atomic (surface disorder as dislocations and steps, chemical inhomogeneities) scale and adsorption phenomena [49,52-55]. Also for the LF time constant n_{ox} results less than 1. This fact may be due to surface heterogeneities [49,52-54], variations of oxide composition, which cause a distribution of resistivity and dielectric constant [54,56], and diffusion phenomena in the oxide film [49,50,54].

The analysis of EIS data shows that for the untreated samples R_{tot} tends to increase according to the

sequence AISI 202 < AISI 316L < P558 (Table 4). When nitriding is performed, a slight decrease in the CPE components and a marked increase in the resistive part related to the oxide layer are observed (Table 4). Thus, an increase of R_{tot} is obtained, suggesting that nitrided samples have a better corrosion resistance, which tends to be higher when the treatment is performed at 380 °C.

The analysis of EIS data for the P558 samples nitrided at 380 °C shows that in the phase angle plot three inflections of the curve are observable, suggesting the presence of three time constants. Thus, a model with three time constants hierarchically connected was chosen (Fig. 10 b), and the corresponding EEC parameter values are reported in Table 5. Models with three time constants have been proposed for inhomogeneous surfaces as those obtained for anodized aluminium [57] or for Ni-based superalloys, having a porous external oxide layer on a compact inner oxide film [58]. Taking into account these models, it may be supposed that R_1 and CPE_1 are related with a porous and/or heterogeneous external oxide layer, R_2 and CPE_2 are related with the processes occurring at the electrode/electrolyte interface, while R_3 and CPE_3 are related with the processes occurring in the inner compact oxide phase. The comparison of R_{tot} value for this sample type is in accordance with the results obtained for the other alloys, i.e. a tendency to a better corrosion resistance.

3.3.3 Potentiodynamic analysis

Representative polarization curves of untreated and nitrided samples, tested in 5 % NaCl aerated solution, are depicted in Fig. 11. The average corrosion potential, passive current density, pitting potential (evaluated as the potential beyond which anodic current density last crossed 5 µA cm^{-2} before the end of the corrosion tests) and charge for unit surface relative to the three chosen potential ranges (zone I, II and III) are reported in Table 6.

For all the sample types the polarization curves are typical of passive materials subjected to localized corrosion beyond a threshold of the potential values.

For the untreated samples no significant difference in the corrosion potential values is observed. Regarding pitting potential, the lowest value is registered for AISI 202 samples, while the highest

13

for P558 ones, as conceivable taking into account the PREN of the alloys. After the tests, the surface of the AISI 316L and AISI 202 samples shows the presence of many large and deep pits, randomly distributed on the surface and having a vertical development, due to the vertical position of the samples during the corrosion tests (Fig. 12 a, b). Moreover, crevice corrosion occurred in the area shielded by the PTFE gasket. On P558 samples only a very shallow groove due to crevice phenomena is observable (Fig. 12 c).

For all the nitrided samples, significantly nobler corrosion potential and lower passive current values are observed in comparison with untreated alloys. For AISI 316L and AISI 202 samples the pitting potential is higher than that of the untreated ones, and tends to increase as the treatment temperature is higher; after this potential value, the anodic current of these sample types remains significantly smaller than that of the untreated ones.

For AISI 316L very high pitting potential values were registered (Fig. 11 a). After the tests the sample surface of 360-°C nitrided samples has a fairly small damage, with a shallow groove due to crevice corrosion (Fig. 12 d). Microscopy observation shows that micrometric and submicrometric pits are present, both inside the grains at the grain boundaries (Fig. 13 a). Regarding the 380-°C treated samples, the surface seems fairly untouched and few very shallow pits are observed (Fig. 12 g). Micrometric pits tend to form in correspondence with grain boundaries and shear lines (Fig. 13 b).

For AISI 202 samples nitrided at 360 °C, the pitting potential is about +710 mV (Ag/AgCl), but the following anodic current values remain still lower that those of the untreated alloy (Fig. 11 b). As a consequence, the damage due to corrosion phenomena is fairly small and only few shallow pits are observed (Fig. 12 e). When the samples are nitrided at 380 °C, after the tests the surface seems fairly untouched and very few shallow pits are present (Fig. 12 h). Microscopy observation shows features similar to those of AISI 316L samples, with micrometric and submicrometric pits that form inside the grains and in correspondence with grain boundaries and shear lines.

Regarding P558, an increase of both corrosion and pitting potential values is observed when the

14

samples are nitrided at 360 °C (Fig. 11 c). After the tests the surface seems to have only minor traces of corrosion phenomena due to crevice (Fig. 12 f). Few micrometric and submicrometric pits are present on the surface (Fig. 13 c). When nitriding is performed at 380 °C, the corrosion potential value is comparable with those of the other alloys. At about +630 mV (Ag/AgCl) anodic current has a fast increase up to about +950 mV (Ag/AgCl) and then it decreases to values typical for a second small passivity branch. After the tests, on the surface a coloured region corresponding to the PTFE gasket is present (Fig. 12 i), suggesting that the main corrosion phenomena are due to crevice; very few shallow pits are observed only on selected samples as that shown in the figure. Many micrometric and submicrometric pits are present, and they tend to develop also along shear lines and grain boundaries (Fig. 13 d).

An increase and a decrease of the anodic current values to delineate a very small current peak are observed also for AISI 316L nitrided at 380 °C, and for P558 untreated and nitrided at 360 °C; the current increase begins at about +630 mV (Ag/AgCl) and the peak is at about +830 mV (Ag/AgCl). The coulometric analysis is in accordance with the potentiodynamic results. For nitrided AISI 316L and AISI 202 samples the charge values of the three zones are significantly smaller in comparison with those of the untreated alloys. Regarding P558 steel, smaller values are recorded only when the samples are nitrided at 360 °C. When nitriding is performed at 380 °C, smaller values are obtained only for zone I, i.e. in the potential range where no significant corrosion phenomena occurred.

3.3.4 Galvanostatic analysis

The typical chronopotentiometric curves of untreated and nitrided samples are depicted in Fig. 14. The potential values corresponding to the maximum (E_{max}) and to the stationary (E_{min}) potential values are reported in Table 7.

The curves for untreated AISI 316L (Fig. 14 a) and AISI 202 (Fig. 14 b) samples show the typical three distinct regions, with a very fast potential increase up to the maximum value (E_{maxI}), a decrease followed by potential fluctuations, which are more noticeable for AISI 202 samples, and

15

then the tendency to reach a stationary value (E_{minI}). After the tests, the surface of the samples shows the presence of a few deep pits (Fig. 15 a, b). It has to be noted that the maximum potential value is higher than E_{pit}, as recorded with the potentiodynamic method (Table 6). The E_{minI} value is higher than E_{corr} for AISI 316L samples, so that it may be hypothesized that pits are able to repassivate if potential is lowered below E_{minI}. On the other hand, for AISI 202 samples E_{minI} is slightly lower than E_{corr}, suggesting that repassivation might not occur.

For untreated P588 samples the potential maximum is reached after a longer time, in comparison with AISI 316L and AISI 202, and only very small fluctuations are observed (Fig. 14 c). After the tests the surface of the samples shows crevice phenomena corresponding to the PTFE gasket and a slight yellow colouring of the surface in the middle of the test area (Fig. 15 c). The very high E_{maxI} and E_{minI} values suggest that not only crevice corrosion but also a transpassive dissolution of the oxide film occurred.

When samples are nitrided, the chronopotentiometric curves have peculiar features. All the sample types show a fast potential increase up to a first maximum (E_{maxI}), and a decrease followed by a further increase towards a second maximum (E_{maxII}). After this maximum, the curves have two different regimes: a first one, in which decreasing potential values still remain very high (Region IIIA) and which can be ascribed to the modified layer. Then, potential has an abrupt decrease and it reaches values comparable with those of the untreated alloy (Region IIIB). For both these regions a stationary potential is not always attained, so the average potentials reported in Table 7 were calculated using the values reached before the transition from Region IIIA to the potential abrupt decrease for E_{minI}, and the values reached at the end of the test for E_{minII}.

Regarding AISI 316L steel (Fig. 14 a), when the samples are nitrided at 360 °C, the first maximum reaches very high values, followed by a moderate decrease (about 50 mV), and then a fairly fast increase towards a higher second maximum. The potential maintains high values with only minor fluctuations and then it decreases to values lower than those measured for the untreated alloy, but significantly higher than the corrosion potential measured for the untreated steel with the

16

potentiodynamic method. After the test, the main corrosion phenomena on the surface of the samples are due to crevice corresponding to the gasket. A very slight colouring of the surface, suggesting the occurrence of a transpassive dissolution of the oxide film, and a few very shallow pits are also observable (Fig. 15 d). Micrometric pits are also present, both inside the grains and along grain boundaries and shear lines (Fig. 16 a).

For 380-°C nitrided samples E_{maxI} is smaller and the time needed for reaching E_{maxII} is longer than for 360-°C treated AISI 316L. Then, many potential fluctuations are present, and they may be ascribed to damages of the modified layer and attempts of repassivation, before potential values comparable with those of the untreated matrix are reached. After the tests, the surface shows significant crevice phenomena together with a few small pits and a very slight colouring (Fig. 15 g); many micrometric pits, as those observed in 360-°C nitrided samples, are also present.

When AISI 202 is considered (Fig. 14 b), the potential of samples nitrided at 360 °C shows many fluctuations after E_{maxII}, suggesting that many activation and repassivation phenomena occurred in the modified layer. When the damage reaches the substrate, significantly lower potential values are recorded, even if fluctuations are still present. These values are higher than those recorded for the untreated samples and in comparison with the corrosion potential as measured with the potentiodynamic method. After the tests, the samples show only a few pits, mainly corresponding to the gasket (Fig. 15 e), together with many micrometric pits, as those observed for AISI 316L samples.

Also the 380-°C treated samples show many fluctuations after E_{maxII}, and very deep minima are present. Marked fluctuations are observed when substrate potential values are reached. After the tests, the surface shows the presence of some pits and a dark colouring where part of the gasket was present (Fig. 15 h). At microscopic level, many pits are present, mainly along grain boundaries and shear lines.

Regarding P558 (Fig. 14 c), for the 360-°C nitrided samples the first maximum is fast reached, followed by a very small decrease and by an increase towards a very high second maximum. Then

the potential values have a very smooth decrease. The transition between the first region (Region IIIA), characteristic of the modified layer, and the second one, characteristic of the matrix, is not as steep as that observed for AISI 316L and AISI 202 samples, and then the potential values show minor fluctuations, but they remain higher than those of the untreated samples. After the tests, the surface shows crevice phenomena, together with a few very shallow pits and a marked yellowish colouring (Fig. 15 f). Many micrometric and submicrometric pits are also observable (Fig. 16 b).

When the samples are treated at 380 °C, the first maximum and, particularly, the second one are reached after a long time. Then, the potential maintains very high values, significantly higher than those of the untreated alloy. No sign of the transition from the Region IIIA to potential values typical of the matrix is detected. After the tests, crevice phenomena are observed and the surface has a yellow colour (Fig. 15 i); at microscopic level pits are also observable. For both nitrided sample types the very high potential values and the surface appearance suggest that transpassive dissolution of the oxide film occurred.

4. Discussion

Nitrogen surface enrichment, performed by means of low temperature nitriding, allows to produce modified surface layers which significantly enhance surface microhardness and corrosion resistance characteristics of austenitic stainless steels, due to the formation of S phase. This phase can be formed not only in alloys in which Ni is present in fairly high amount, as in AISI 300 and AISI 200 series stainless steels, but also in a steel, as P558, in which Ni is negligible. This observation was made also by Buhagiar et al. [31], but they did not succeed in producing a nitride-free modified layer. In this research we showed that also in a nickel-free stainless steel it is possible to obtain S phase without the precipitation of nitrides, as in the 360-°C nitrided P558 samples.

For all steel types, the modified surface layers have a double layer microstructure. This microstructure, previously observed in AISI 300 [20,21,29,33,59-61] and AISI 200 [20,29,33] series stainless steels, consists of an outer layer, in which S phase is present, and an inner layer, in

which an austenite with a slightly expanded lattice parameter is detected. This latter phase, here indicated as $\gamma(N, C)$, has been hypothesized to be due to an accumulation of carbon atoms at the end of nitrogen profile [59], or to the presence of nitrogen atoms which are not trapped by chromium [60], or to be related to the high residual stresses induced between the S phase layer and the substrate [61]. Another peculiar feature of the modified layers is the formation of shear bands and ε_N' martensite in the outer layer, which are related to the plastic deformation due to the formation of the modified surface layers and to the alloy composition [20,21,29,43]. As previously observed [29], AISI 202 has a higher tendency to form shear bands and ε_N' martensite in comparison with AISI 316L. For P558 steel, the high yield strength of this steel, which can be supposed on the basis of microhardness measurements and literature data [62], delays the plastic deformation and the appearance of shear bands, which become well observable only when the samples are nitrided at 380 °C. The peculiar surface features, due to local plastic deformation, and plasma etching during nitriding cause an increase of surface roughness, as previously observed [41]. The distance between peaks and valleys on the surface tends to increase, so an increase of Rz and Rc parameters, and of the average roughness Ra, is registered for all the nitrided samples, in comparison with the untreated ones. The roughness values have a good agreement with morphology observations: when more shear bands form in addition to surface etching, as for the 380-°C nitrided samples, an increase of surface roughness is observed. The local plastic deformation, promoted by the solubilization of a large nitrogen amount, is also strictly related to the formation of h.c.p. ε' martensite, induced by the occurrence of wide stacking faults in the f.c.c. lattice [29,63]. In the nitrided austenitic stainless steels, nitrogen atoms may remain entrapped in the h.c.p. structure, causing a lattice expansion. This nitrogen induced martensite, ε_N', is hypothesized to be the precursor of h.c.p. ε-nitride, which maintains the h.c.p. arrangement of the substitutional atoms and it has an ordering of N atoms [44]. The formation of ε-nitride depends on both treatment conditions and steel composition [20,29]. On the basis of a previous study [29], it may be supposed that, for

AISI 316L and AISI 202, nitrides are not able to form at the temperatures used in the present research. On the other hand, P558 contains high amounts of manganese and molybdenum together with chromium, which are all strong nitride forming elements, so the precipitation of nitrides when $\varepsilon_N{'}$ forms in large amounts, as at 380 °C, cannot be ruled out, even if an ordering of nitrogen atoms was not observed with XRD analysis.

For all the examined stainless steels nitriding has a significant effect on corrosion behaviour in NaCl solution. The formation of an outer layer consisting mainly of S phase is able to promote a higher resistance to corrosion, in comparison with the untreated steels, as evidenced by EIS analysis. Corrosion potential values increase and passive anodic current values tend to decrease, in accordance with previous observations [20,24,29,33]. Both potentiodynamic and galvanostatic tests suggest that the potential, at which localized corrosion phenomena occur, is higher than that of untreated steels, and that, as long as the modified layers are not completely crossed by corrosion, the layers may exert their protective action.

Nitriding conditions influence the corrosion behaviour. For AISI 316L and AISI 202 stainless steels, nitriding at 380 °C allows to produce surface layers which have a higher corrosion resistance than that of the samples treated at 360 °C, as suggested by the increasing of resistance R_{tot} and of the different evaluated potential parameters (E_{corr}, E_{pit}, E_{max}, E_{min}). It may be supposed that this behaviour is due to higher nitrogen content and thickness of the modified surface layers, in accordance with our previous results [33,48].

When the alloy composition is taken into account, the comparison of the results obtained with the different steels suggests that the corrosion potential and the passive anodic current before the occurrence of localized corrosion phenomena are influenced mainly by solubilized nitrogen, and the alloy elements play only a minor role. This result is in accordance with our previous studies [29,33], but not with those of other authors [25,28], which found different E_{corr} values for different steels after nitriding. The results of these authors may have been influenced by the fairly short delay time (5 min [28], 30 min [25]) before potentiodynamic tests.

The increase of potential scans up to +1200 mV (Ag/AgCl) in the potentiodynamic tests, instead of +1000 mV (Ag/AgCl) [29,33], and the use of galvanostatic technique allow to put in evidence that the potential, at which localized corrosion phenomena occur, is influenced by both nitrogen content and alloy elements. Beyond the beneficial effect of nitrogen, the high corrosion resistance observed for nitrided AISI 316L and P558 also at high anodic potentials may be ascribed to the presence of Mo in these steels. Mo is able to enhance pitting corrosion resistance, and it is supposed to have effect in both delaying the attack of Cl$^-$ ions on the passive film and improving repassivation [64-66]. By means of a synergistic action, Mo and N are able to improve corrosion resistance to localized phenomena (pitting, crevice) in chloride-ion containing solutions further on, when media with acidic or neutral conditions are present, as observed by other authors [10,25,66]. As a consequence, the corrosion resistance of the examined austenitic stainless steels after nitriding tends to maintain the same trend of untreated steels, i.e. AISI 202 < AISI 316L < P558, when only a small amount of ε_N' forms, as with the treatment at 360 °C. For the samples nitrided at 380 °C, Mo and N action allows to increase the corrosion resistance of AISI 316L further on in comparison with AISI 202. For P558 steel, Mo and N act only in part for increasing corrosion resistance. This sample type has a higher corrosion potential than the untreated steels, but it is subjected to larger damage due to crevice and pitting in comparison with 360-°C nitrided samples. The presence of an anodic current peak at +950 mV (Ag/AgCl) and a second passivity branch suggests the occurrence of oxidation phenomena which may be promoted by the heterogeneous structure formed by S phase and the fairly large amount of h.c.p. phase (ε_N' martensite and/or nitride precipitates). A similar but smaller anodic current peak at comparable potentials was observed in our previous papers for nitrided AISI 202, AISI 304L and AISI 316L samples [29,33], when small amounts of nitrides (ε-nitride and CrN), together with ε_N' martensite, were able to form. The very small anodic current peak at about +830 mV (Ag/AgCl), observed in the present paper for AISI 316L nitrided at 380 °C, and for P558 untreated and nitrided at 360 °C, was also detected in an our previous research for 380-°C nitrided AISI 202 samples and 400-°C nitrided AISI 316L samples [33]. A more marked peak at this

potential was observed for a 22Cr-18Mn-0.83N high nitrogen nickel-free austenitic stainless steel subjected to different rolling strains and tested in a 3.5 % NaCl solution [67]. The potential value, corresponding to the current increase for the peaks detected in the present research, is about +630 mV (Ag/AgCl). On the basis of the Pourbaix diagram for a Cr-Mn-Mo steel [65], for an acidic solution, as the one expected for pitting or crevice phenomena, the oxidation of Cr^{3+}, in form of Cr_2O_3, to Cr^{6+}, as soluble $Cr_2O_7^{2-}$, might be supposed. At this potential value also the transformation of MoO_3 into soluble MoO_4^{2-} might occur, but the fact that the anodic peak is observed also for stainless steels, which do not contain Mo, as AISI 202 [29,33], AISI 304L [29], and the 22Cr-18Mn-0.83N stainless steel [67], suggests that Cr oxidation plays the major role. At higher potentials also Mn might contribute to the current peak, with the oxidation of Mn^{4+}, as MnO_2, to Mn^{7+}, as soluble MnO_4^-. The fact that the maximum of the current peak is observed at higher potential when ε_N' martensite and/or nitride precipitates form, as for the 380-°C nitrided P558 samples, might be due to a more difficult repassivation where corrosion phenomena occur. Further analysis will be performed in order to elucidate this point.

It is interesting to note that for all the samples the potential, at which localized corrosion phenomena begin, is higher for galvanostatic tests in comparison with that evaluated with potentiodynamic polarization. Moreover, galvanostatic tests suggest that, for the modified layers, the potential below which corrosion does not happen is higher than E_{corr}, so that it may be hypothesized that repassivation phenomena may occur when the depth of pits or crevices is not too high. On the contrary, when the cyclic potentiodynamic method was used, the repassivation, or protection, potential was not measured [22], or it was lower than that of the untreated steel [68]. These different results may be ascribed to the used test techniques and their experimental parameters, which influence the damage extent, and thus the system response [35,69,70].

5. Conclusions

Low temperature glow-discharge nitriding, performed at 360 and 380 °C at 340 Pa for 3 h, is able to

produce modified surface layers, consisting mainly of S phase and without the formation of large amounts of nitrides, not only on AISI 316L and AISI 202 austenitic stainless steels, but also on the nickel-free P558 alloy. These layers allow to significantly enhance surface microhardness, in comparison with the untreated steels.

The study of the corrosion behaviour of nitrided and untreated samples, tested in a 5 % NaCl aerated solution, puts in light that the nobler corrosion potentials and lower anodic passive currents of the nitrided samples may be influenced mainly by solubilized nitrogen. When the potential, at which localized phenomena occur, is taken into account, also alloy elements may be supposed to play an important role. In particular, Mo, in synergy with N, acts to improve corrosion resistance further on, so that the corrosion resistance of the tested nitrided steels tends to maintain the same trend of untreated steels, i.e. AISI 202 < AISI 316L < P558, when only a small amount of nitrogen induced ε_N' martensite is present, as with the 360-°C treatment. When a fairly large amount of h.c.p. phase (ε_N' and/or nitrides) is able to form on P558 steel, as with the nitriding at 380 °C, Mo and N are able to counteract corrosion phenomena only in part, probably due to the heterogeneous structure of the surface.

References

[1] K.H. Lo, C.H. Shek, J.K.L. Lai, Recent developments in stainless steels, Mater. Sci. Eng. R 65 (2009) 39-104.

[2] S.N. Ghali, Low Carbon High Nitrogen Low Nickel Stainless Steel, Steel Research Int. 84 (2013) 450-456.

[3] H. Hänninen, J. Romu, R. Ilola, J. Tervo, A. Laitinen, Effects of processing and manufacturing of high nitrogen-containing stainless steels on their mechanical, corrosion and wear properties, J. Mater. Process. Tech. 117 (2001) 424-430.

[4] H. Baba, T. Kodama, Y. Katada, Role of nitrogen on the corrosion behavior of austenitic stainless steels, Corros. Sci. 44 (2002) 2393-2407.

[5] U.K. Mudali, S. Ningshen, Corrosion properties of nitrogen bearing stainless steels, in: U.K. Mudali and B. Raj (Eds.), High Nitrogen Steels and Stainless Steels - Manufacturing Properties and Applications, Alpha Science International Ltd, Pangbourne, UK, 2004, pp. 133-181.

[6] M.O. Speidel, Corrosion Science of Stainless Steels, in: Proceedings of International Conference on Stainless Steels (Stainless Steels '91), Iron and Steel Institute of Japan, Tokyo, 1991, pp. 25-35.

[7] M. Metikoš-Huković, R. Babić, Z. Grubač, Ž. Petrović, N. Lajçi, High corrosion resistance of austenitic stainless steel alloyed with nitrogen in an acid solution, Corr. Sci. 53 (2011) 2176-2218.

[8] K. Zagorski, A. Doraczynska, Potentiodynamic polarization behaviour of two 17Cr-13Ni-2.5Mo austenitic steels with different N contents, Corros. Sci. 16 (1976) 405-410.

[9] A. Belfrouh, C. Masson, D. Vouagner, A.M. De Becdelievre, N.S. Prakash, A.P. Audouard, The cumulative effect of alloying elements N, W, Mo and Cu on the corrosion behaviour of 17Cr–13Ni stainless steel in 2 N H_2SO_4, Corros. Sci. 38 (1996) 1639-1648.

[10] R.F.A. Jargelius-Pettersson, Electrochemical investigation of the influence of nitrogen alloying on pitting corrosion of austenitic stainless steels, Corros. Sci. 41 (1999) 1639-1664.

[11] I. Olefjord, L. Wergrelius, The influence of nitrogen on the passivation of stainless steels, Corros. Sci. 38 (1996) 1203-1220.

[12] H. Baba, Y. Katada, Effect of nitrogen on crevice corrosion in austenitic stainless steel, Corros. Sci. 48 (2006) 2510-2524.

[13] M.B. Ives, Y.C. Lu, JL. Luo, Cathodic reactions involved in metallic corrosion in chlorinated saline environments, Corros. Sci. 32 (1991) 91-102.

[14] C.R. Clayton, L. Rosenzweig, M. Oversluizen, Y.C. Lu, The influence of nitrogen on the passivity of 18-8 (0.24%N) stainless steels, in: E. McCafferty and R.J. Brodd (Eds.), Surfaces, Inhibition and Passivation, The Electrochemical Society, Pennington, NJ, 1986, pp. 323-339.

[15] S. Ningshen, U. Kamachi Mudali, V.K. Mittal, H.S. Khatak, Semiconducting and passive film properties of nitrogen-containing type 316LN stainless steels, Corros. Sci. 49 (2007) 481-496.

[16] L. Vehovar, A. Vehovar, M. Metikos-Hukovic, M. Tandler, Investigations into the stress corrosion cracking of stainless steel alloyed with nitrogen, Mater. Corros. 53 (2002) 316-327.

[17] F.M. Bayoumi, W.A. Ghanem, Effect of nitrogen on the corrosion behavior of austenitic stainless steel in chloride solutions, Mater. Lett. 59 (2005) 3311-3314.

[18] H. Dong, S-phase surface engineering of Fe-Cr, Co-Cr and Ni-Cr alloys, Int. Mater. Rev. 55 (2010) 65-98.

[19] T. Bell, Surface engineering of austenitic stainless steel, Surf. Eng. 18 (2002) 415-422.

[20] A. Fossati, E. Galvanetto, T. Bacci, F. Borgioli, Improvement of corrosion resistance of austenitic stainless steels by means of glow-discharge nitriding, Corros. Rev. 29 (2011) 209-221.

[21] T. Christiansen, M.A.J. Somers, Low temperature gaseous nitriding and carburising of stainless steel, Surf. Eng. 21 (2005) 445-455.

[22] X.M. Zhu, M.K. Lei, Pitting corrosion resistance of high nitrogen f.c.c. phase in plasma source ion nitrided austenitic stainless steel, Surf. Coat. Technol. 131 (2000) 400-403.

[23] I. Flis-Kabulska, Y. Sun, J. Flis, Monitoring the near-surface pH to probe the role of nitrogen in corrosion behaviour of low-temperature plasma nitrided 316L stainless steel, Electrochim. Acta 104 (2013) 208-215.

[24] M.K. Lei, X.M. Zhu, In vitro corrosion resistance of plasma source ion nitrided austenitic stainless steels, Biomaterials 22 (2001) 641-647.

[25] P. Saravanan, V.S. Raja, S. Mukherjee, Effect of alloyed molybdenum on corrosion behavior of plasma immersion nitrogen ion implanted austenitic stainless steel, Corr. Sci. 74 (2013) 106-115.

[26] M. Egawa, N. Ueda, K. Nakata, M. Tsujikawa, M. Tanaka, Effect of additive alloying element on plasma nitriding and carburizing behavior for austenitic stainless steels, Surf. Coat. Technol. 205 (2010) S246-S251.

[27] K. Köster, P. Kaestner, G. Bräuer, H. Hoche, T. Troßmann, M. Oechsner, Material condition tailored to plasma nitriding process for ensuring corrosion and wear resistance of austenitic stainless steel, Surf. Coat. Technol. 228 (2013) S615-S618.

[28] J. Buhagiar, H. Dong, Corrosion properties of S-phase layers formed on medical grade austenitic stainless steel, J. Mater. Sci.: Mater. Med. 23 (2012) 271-281.

[29] F. Borgioli, E. Galvanetto, T. Bacci, Low temperature nitriding of AISI 300 and 200 series austenitic stainless steels, Vacuum, 127 (2016) 51-60.

[30] Y. Gao, S. Zheng, Effect of plasma nitriding temperatures on characteristics of AISI 201 austenitic stainless steel, Surf. Rev. Lett. 23 (2016) 1550084.

[31] J. Buhagiar, X. Li, H. Dong, Formation and microstructural characterisation of S-phase layers in Ni-free austenitic stainless steels by low-temperature plasma surface alloying, Surf. Coat. Technol. 204 (2009) 330-335.

[32] J. Buhagiar, Plasma surface engineering and characterisation of biomedical stainless steels, PhD thesis, University of Birmingham, Department of Metallurgy and Materials, Faculty of Engineering, UK, 2008.

[33] F. Borgioli, A. Fossati, L. Raugei, E. Galvanetto, T. Bacci, Low temperature glow-discharge nitriding of stainless steels, in: Proceedings of the 7th European Stainless Steel Conference - Science and Market, Como (Italy), September 21-23, 2011, Associazione Italiana di Metallurgia, Milan, 2011 (CD-rom; ISBN: 978-88-85298-84-2).

[34] A.S. Bondarenko, G.A. Ragoisha, Inverse Problem in Potentiodynamic Electrochemical Impedance, in: A.L. Pomerantsev (Ed.), Progress in Chemometrics Research, Nova Science Publishers, Inc., New York, 2005, pp. 89-102.

[35] S. Frangini, N. De Cristofaro, Analysis of the galvanostatic polarization method for determining reliable pitting potentials on stainless steels in crevice-free conditions, Corr. Sci. 45 (2003) 2769-2786.

[36] J. Landoulsi, C. Dagbert, C. Richard, R. Sabot, M. Jeannin, K. El Kirat, S. Pulvin, Enzyme-induced ennoblement of AISI 316L stainless steel: Focus on pitting corrosion behavior, Electrochim. Acta 54 (2009) 7401-7406.

[37] B. Tzaneva, Effect of pH on the corrosion behaviour of high nitrogen stainless steel in chloride medium, J. Chem. Technol. Metall. 48 (2013) 383-390.

[38] N. Ebrahimi, P. Jakupi, J.J. Noël, D.W. Shoesmith, The Role of Alloying Elements on the Crevice Corrosion Behavior of Ni-Cr-Mo Alloys, Corrosion 71 (2015) 1441-1451.

[39] N. Ebrahimi, J.J. Noël, M.A. Rodríguez, D.W. Shoesmith, The self-sustaining propagation of crevice corrosion on the hybrid BC1 Ni–Cr–Mo alloy in hot saline solutions, Corr. Sci. 105 (2016) 58-67.

[40] B.R. Tzaneva, The influence of temperature on the corrosion behaviour of high nitrogen austenitic stainless steel in chloride media, Bulg. Chem. Commun. 46 (2014) 378-383.

[41] Francesca Borgioli, Emanuele Galvanetto, Tiberio Bacci, Influence of surface morphology and roughness on water wetting properties of low temperature nitrided austenitic stainless steels, Mater. Char. 95 (2014) 278-284.

[42] M.K. Lei, Phase transformations in plasma source ion nitrided austenitic stainless steel at low temperature, J. Mater. Sci. 34 (1999) 5975-5982.

[43] W. Liang, X. Xiaolei, X. Jiujun, S. Yaqin, Characteristics of low pressure plasma arc source ion nitrided layer on austenitic stainless steel at low temperature, Thin Solid Films 391 (2001) 11-16.

[44] M.K. Lei, Y. Huang, Z.L. Zhang, *In situ* transformation of nitrogen-induced h.c.p. martensite in plasma source ion-nitrided austenitic stainless steel, J. Mater. Sci. Lett. 17 (1998) 1165-1167.

[45] K.V. Rybalka, V.S. Shaldaev, L.A. Beketaeva, A.N. Malofeeva, A.D. Davydov, Development of Pitting Corrosion of Stainless Steel 403 in Sodium Chloride Solutions, Russ. J. Electrochem. 46 (2010) 196-204.

[46] S. Jin, A. Atrens, Passive Films on Stainless Steels in Aqueous Media, Appl. Phys. A 50 (1990) 287-300.

[47] C.-O.A. Olsson, D. Landolt, Passive films on stainless steels - chemistry, structure and growth, Electrochim. Acta 48 (2003) 1093-1104.

[48] A. Fossati, F. Borgioli, E. Galvanetto, T. Bacci, Corrosion resistance properties of glow-discharge nitrided AISI 316L austenitic stainless steel in NaCl solutions, Corr. Sci. 48 (2006) 1513-1527.

[49] S. Omanovic, S.G. Roscoe, Electrochemical Studies of the Adsorption Behavior of Bovine Serum Albumin on Stainless Steel, Langmuir 15 (1999) 8315-8321.

[50] Z. Bou-Saleh, A. Shahryari, S. Omanovic, Enhancement of corrosion resistance of a biomedical grade 316LVM stainless steel by potentiodynamic cyclic polarization, Thin Solid Films 515 (2007) 4727-4737.

[51] C.M. Abreu, M.J. Cristóbal, P. Merino, X.R. Nóvoa, G. Pena, M.C. Pérez, Electrochemical behaviour of an AISI 304L stainless steel implanted with nitrogen, Electrochim. Acta 53 (2008) 6000-6007.

[52] E. Navarro-Flores, Z. Chong, S. Omanovic, Characterization of Ni, NiMo, NiW and NiFe electroactive coatings as electrocatalysts for hydrogen evolution in an acidic medium, J. Mol. Catal. A-Chem. 226 (2005) 179-197.

[53] X. Sheng, Y.-P. Ting, S.O. Pehkonen, The influence of sulphate-reducing bacteria biofilm on the corrosion of stainless steel AISI 316, Corr. Sci. 49 (2007) 2159-2176.

[54] J.-B. Jorcin, M.E. Orazem, N. Pébère, B. Tribollet, CPE analysis by local electrochemical impedance spectroscopy, Electrochim. Acta 51 (2006) 1473-1479.

[55] P. Córdoba-Torres, T.J. Mesquita, O. Devos, B. Tribollet, V. Roche, R.P. Nogueira, On the intrinsic coupling between constant-phase element parameters α and Q in electrochemical impedance spectroscopy, Electrochim. Acta 72 (2012) 172-178.

[56] B. Hirschorn, M.E. Orazem, B. Tribollet, V. Vivier, I. Frateur, M. Musiani, Constant-Phase-Element Behavior Caused by Resistivity Distributions in Films II. Applications, J. Electrochem. Soc. 157 (2010) C458-C463.

[57] K. Jüttner, Electrochemical impedance spectroscopy (EIS) of corrosion processes on inhomogeneous surfaces, Electrochim. Acta 35 (1990) 1501-1508.

[58] H. Bai, F. Wang, Protective Properties of High Temperature Oxide Films on Ni-based Superalloys in 3.5% NaCl Solution, J. Mater. Sci. Technol. 23 (2007) 541-546.

[59] T. Michler, Influence of plasma nitriding on hydrogen environment embrittlement of 1.4301 austenitic stainless steel, Surf. Coat. Technol. 202 (2008) 1688-1695.

[60] T. Christiansen, K.V. Dahl, M.A.J. Somers, Nitrogen diffusion and nitrogen depth profiles in expanded austenite: Experimental assessment, numerical simulation and role of stress, Mater. Sci. Tech. 24 (2008) 159-167.

[61] D.L. Williamson, J.A. Davis, P.J. Wilbur, Effect of austenitic stainless steel composition on low-energy, high-flux, nitrogen ion beam processing, Surf. Coat. Technol. 103-104 (1998) 178-184.

[62] U.I. Thomann, P.J. Uggowitzer, Wear–corrosion behavior of biocompatible austenitic stainless steels, Wear 239 (2000) 48-58.

[63] J. Talonen, H. Hänninen, Formation of shear bands and strain-induced martensite during plastic deformation of metastable austenitic stainless steels, Acta Mater. 55 (2007) 6108-6118.

[64] A. Pardo, M.C. Merino, A.E. Coy, F. Viejo, R. Arrabal, E. Matykina, Pitting corrosion behaviour of austenitic stainless steels – combining effects of Mn and Mo additions, Corr. Sci. 50 (2008) 1796-1806.

[65] K.L. Chao, H.Y. Liao, J.J. Shyue, S.S. Lian, Corrosion Behavior of High Nitrogen Nickel-Free Fe-16Cr-Mn-Mo-N Stainless Steel, Metall. Mater. Trans. 45B (2014) 381-391.

[66] C. Loable, I.N. Viçosa, T.J. Mesquita, M. Mantel, R.P. Nogueira, G. Berthom, E. Chauveau, V. Roche, Synergy between molybdenum and nitrogen on the pitting corrosion and passive film resistance of austenitic stainless steels as a pH-dependent effect, Mater. Chem. Phys. 186 (2017) 237-245.

[67] S. Sun, S. Wei, G. Wang, Z. Jiang, J. Lian, C. Ji, The Synthesis and Electrochemical Behavior of High-Nitrogen Nickel-Free Austenitic Stainless Steel, J. Mater. Eng. Perform. 23 (2014) 3957-3962.

[68] S. Picard, J.B. Memet, R. Sabot, J.L. Grosseau-Poussard, J.P. Rivière, R. Meilland, Corrosion behaviour, microhardness and surface characterisation of low energy, high current ion implanted austenitic stainless steel, Mater. Sci. Eng. A 303 (2001) 163-172.

[69] B.E. Wilde, A Critical Appraisal of Some Popular Laboratory Electrochemical Tests for Predicting the Localized Corrosion Resistance of Stainless Alloys in Sea Water, Corrosion 28 (1972) 283-291.

[70] B.E. Wilde, E. Williams, The use of current/voltage curves for the study of localized corrosion and passivity breakdown on stainless steels in chloride media, Electrochim. Acta 16 (1971) 1971-1985.

Figure captions

Fig. 1. Surface morphology of AISI 316L (a), AISI 202 (b) and P558 (c) samples nitrided at 360 °C.
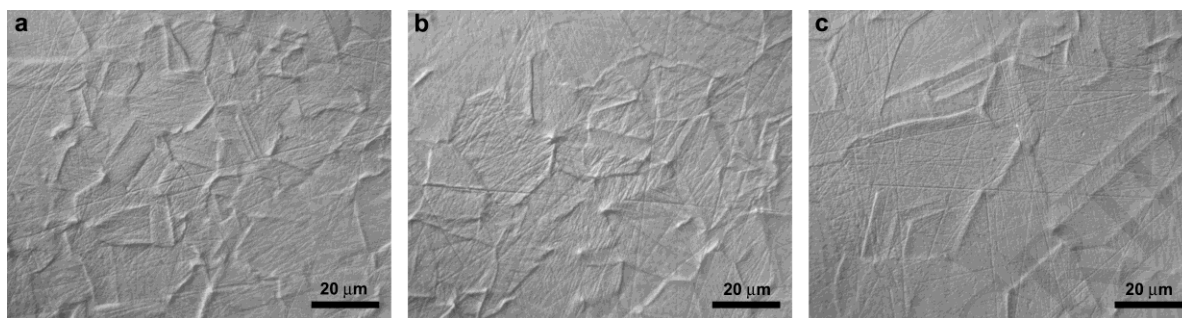
Fig. 2. Micrographs of the modified surface layers of AISI 316L (a), AISI 202 (b) and P558 (c) samples nitrided at 360 °C. (Cross-section; etchant: acetic glyceregia).
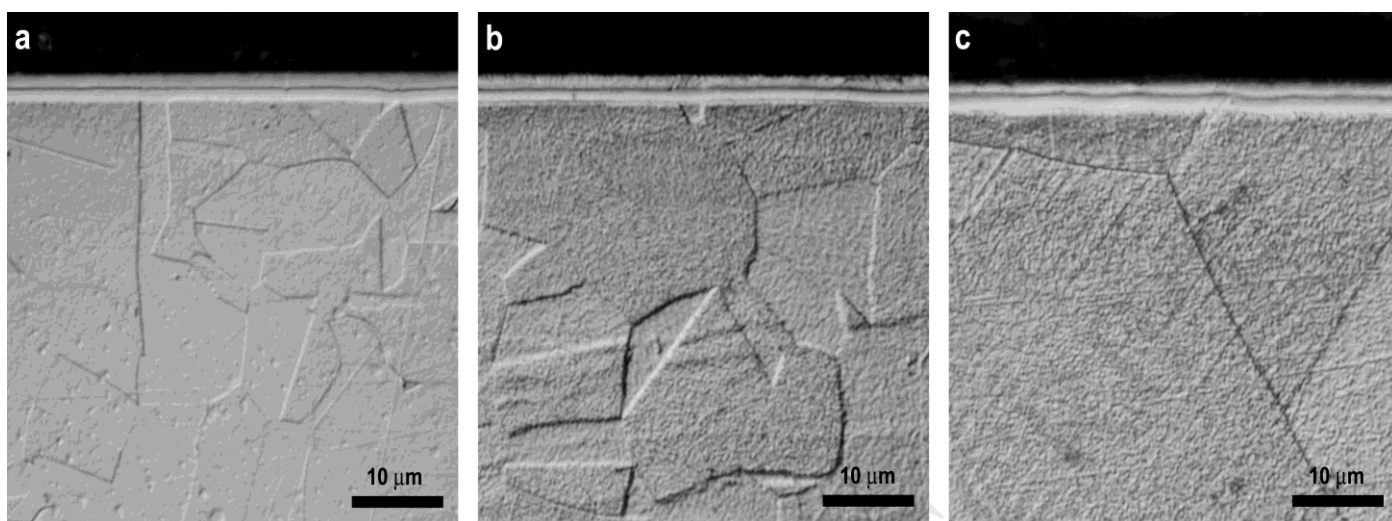
Fig. 3. X-ray diffraction patterns of AISI 316L (a), AISI 202 (b) and P558 (c) samples nitrided at 360 °C (configuration: 10°-incident angle).
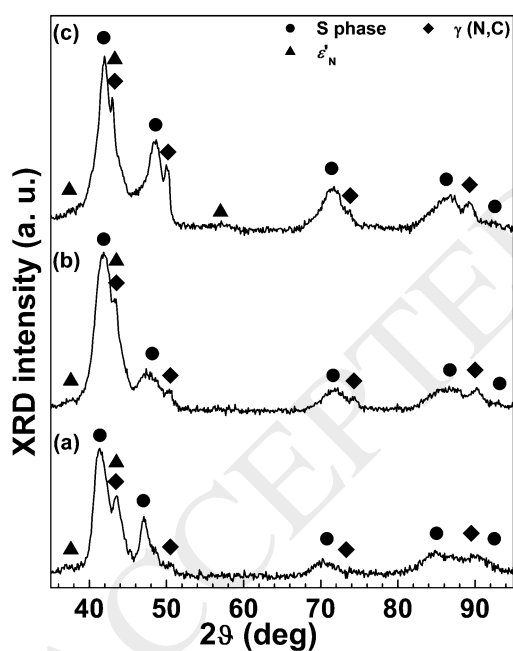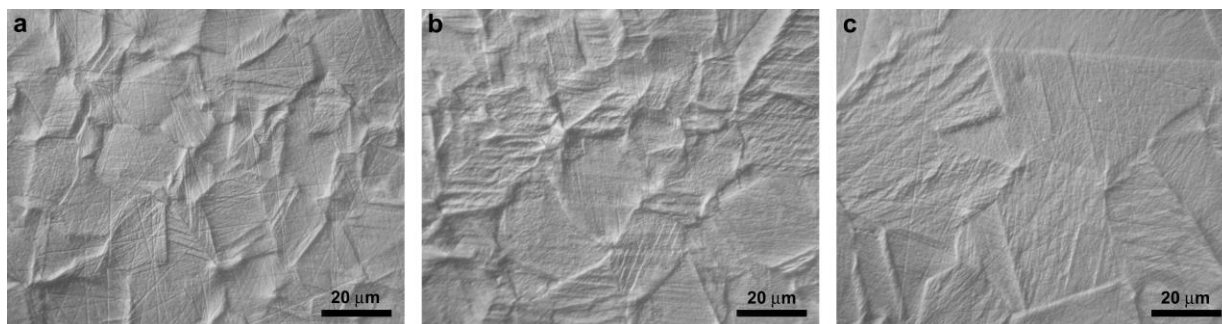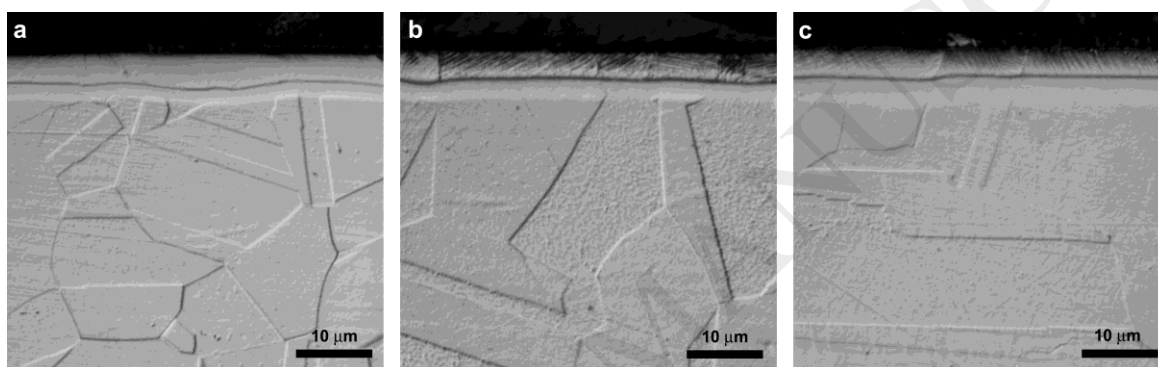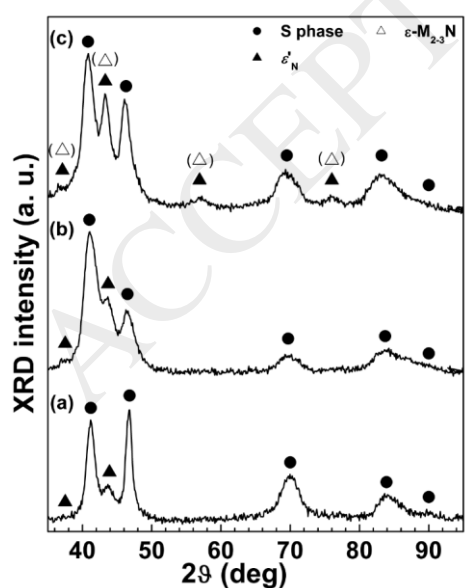
Fig. 4. Surface morphology of AISI 316L (a), AISI 202 (b) and P558 (c) samples nitrided at 380 °C.

Fig. 5. Micrographs of the modified surface layers of AISI 316L (a), AISI 202 (b) and P558 (c) samples nitrided at 380 °C. (Cross-section; etchant: acetic glyceregia).

Fig. 6. X-ray diffraction patterns of AISI 316L (a), AISI 202 (b) and P558 (c) samples nitrided at 380 °C (configuration: 10°-incident angle).

Fig. 7. Surface Knoop microhardness values of AISI 316L, AISI 202 and P558 samples untreated (untr.) and nitrided at 360 °C (360) and 380 °C (380) (test loads: 25, 50 and 100 gf).
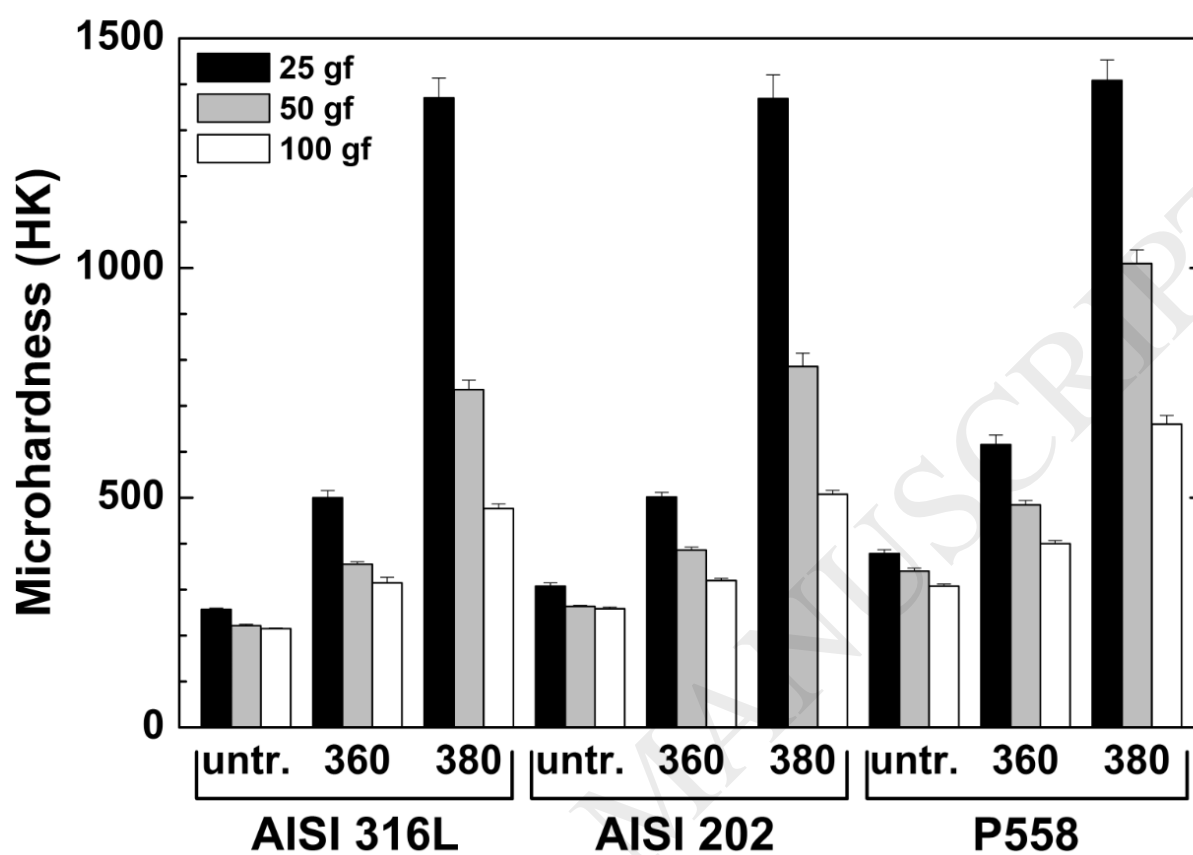
Fig. 8. Open Circuit Potential vs. time for AISI 316L (a), AISI 202 (b) and P558 (c) samples untreated and nitrided at the indicated temperatures (solution: 5 % NaCl, aerated).
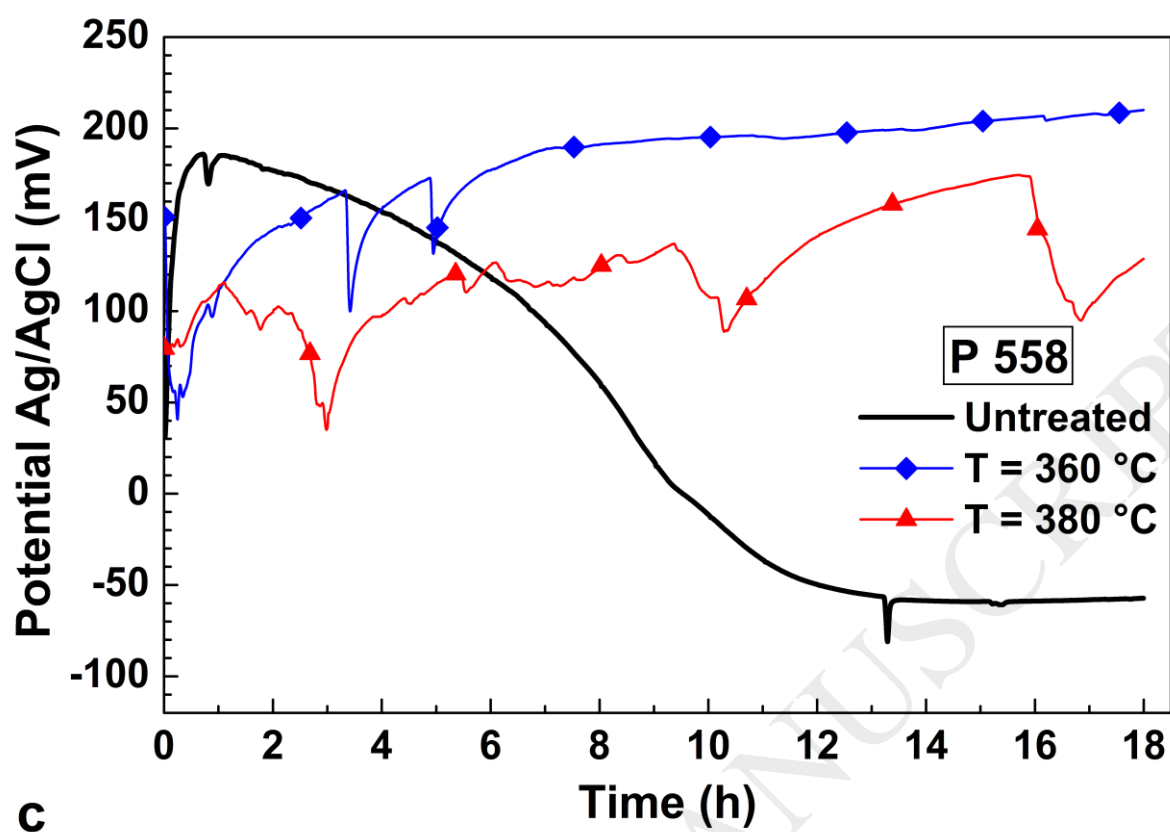

a

b

c
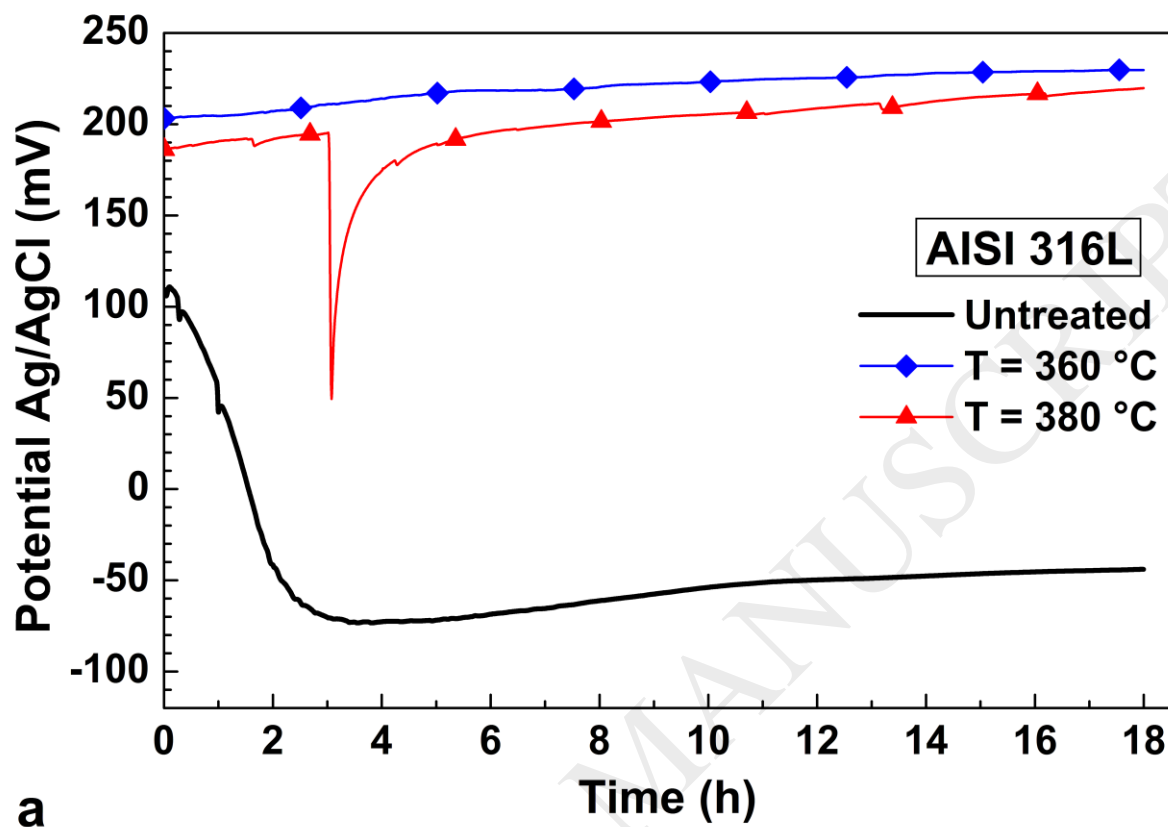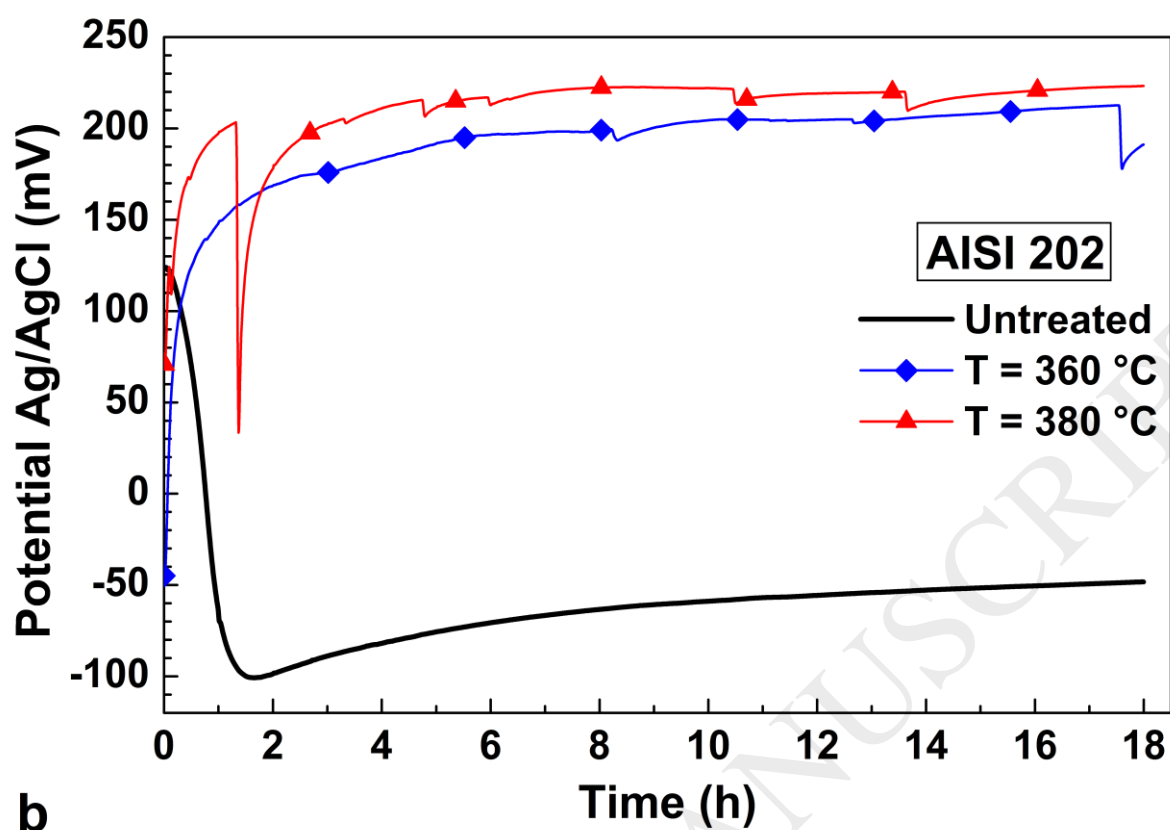
Fig. 9. Bode and Nyquist plots of AISI 316L (a, b), AISI 202 (c, d) and P558 (e, f) samples untreated and nitrided as indicated, recorded at the respective OCP values (solution: 5 % NaCl, aerated). Symbols: experimental data; lines: modelled data obtained using the equivalent electrical circuits of Fig. 10 as explained in the text.
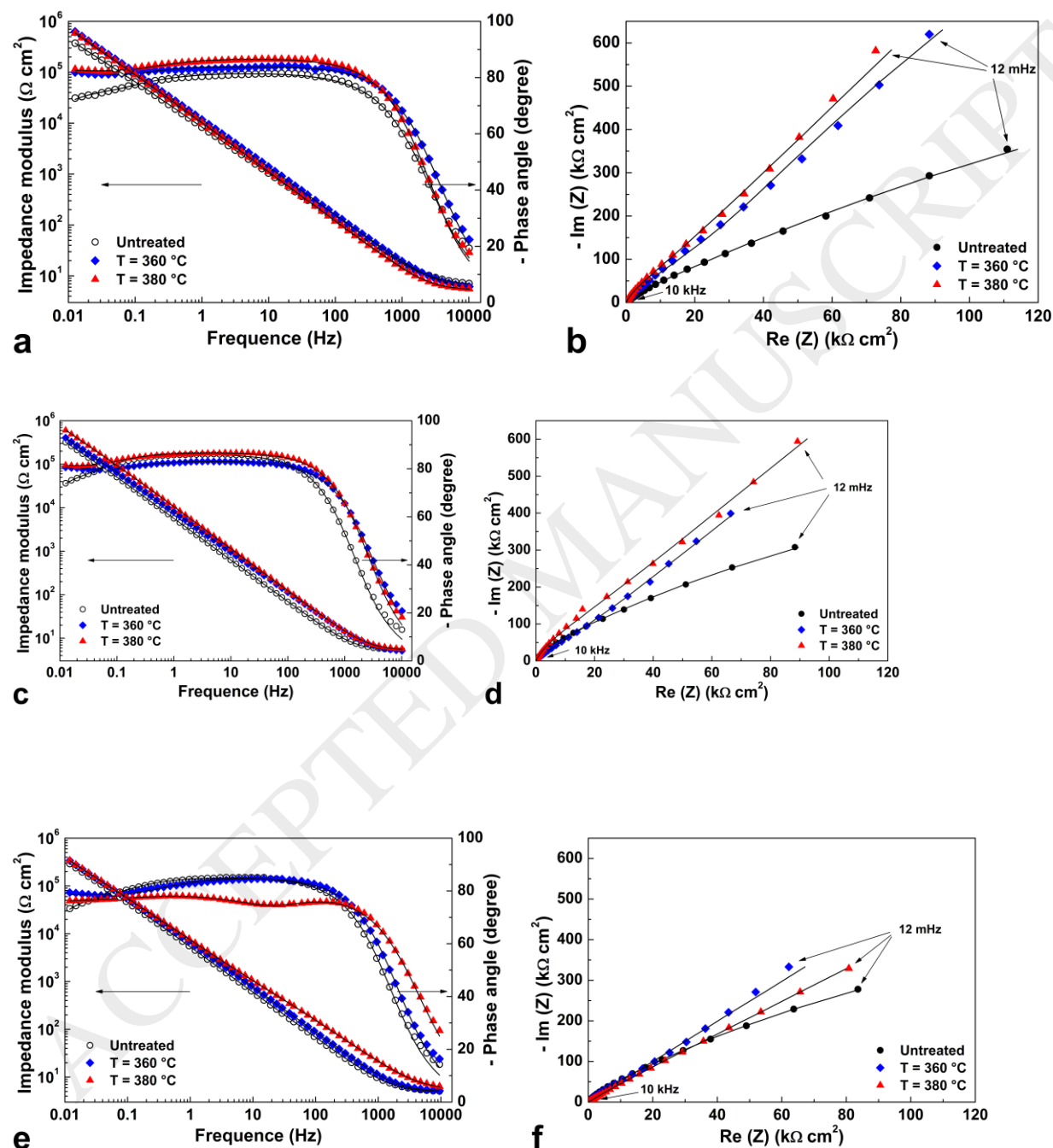
Fig. 10. Electrical equivalent circuits used for quantitative evaluation of EIS spectra. (a): for untreated and 360-°C nitrided samples, and for 380-°C nitrided AISI 316L and AISI 202 samples; (b): for 380-°C nitrided P558 samples.
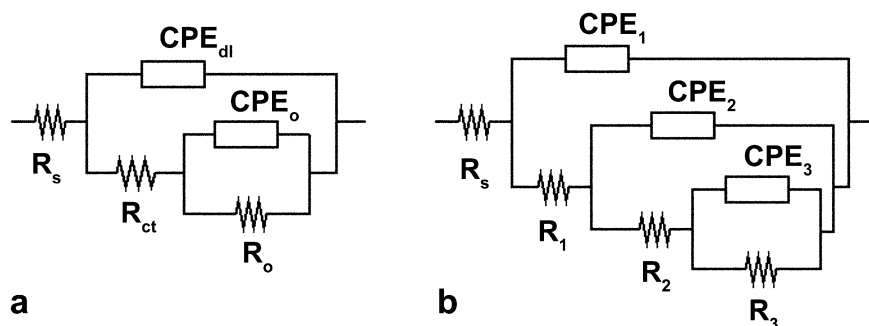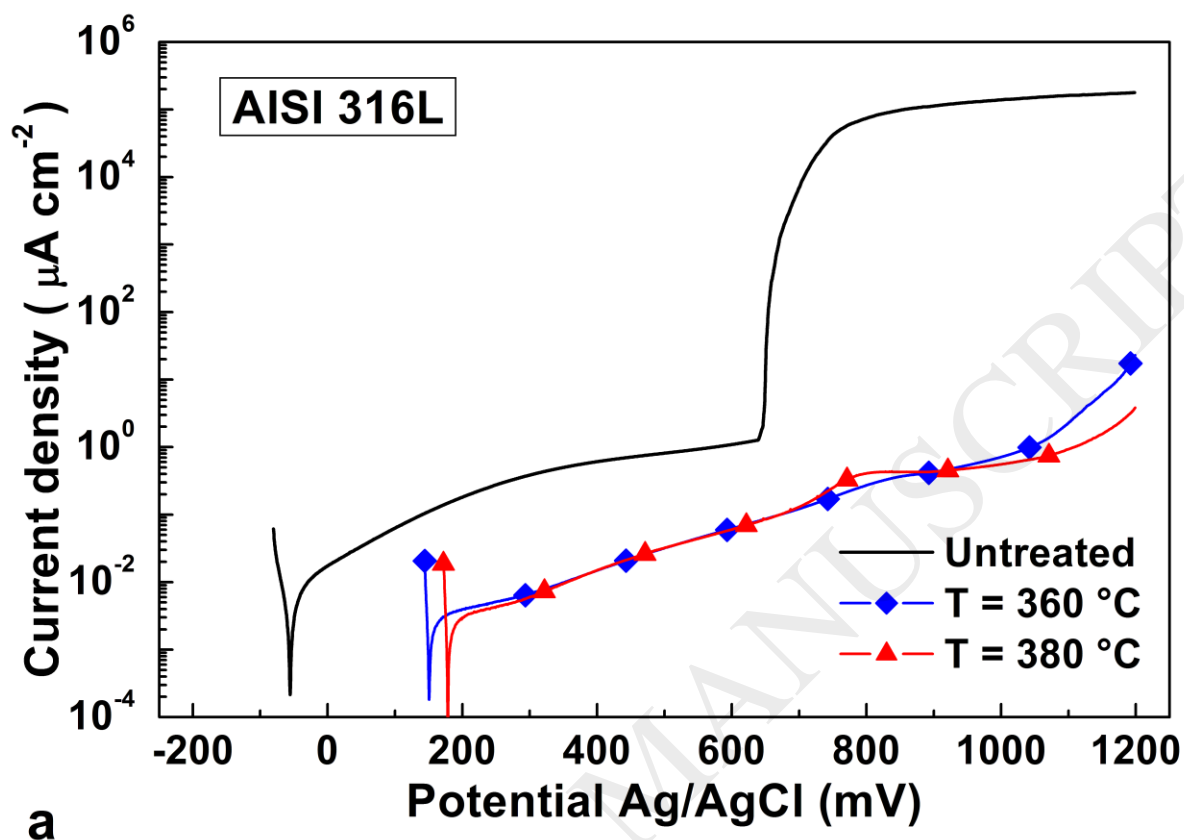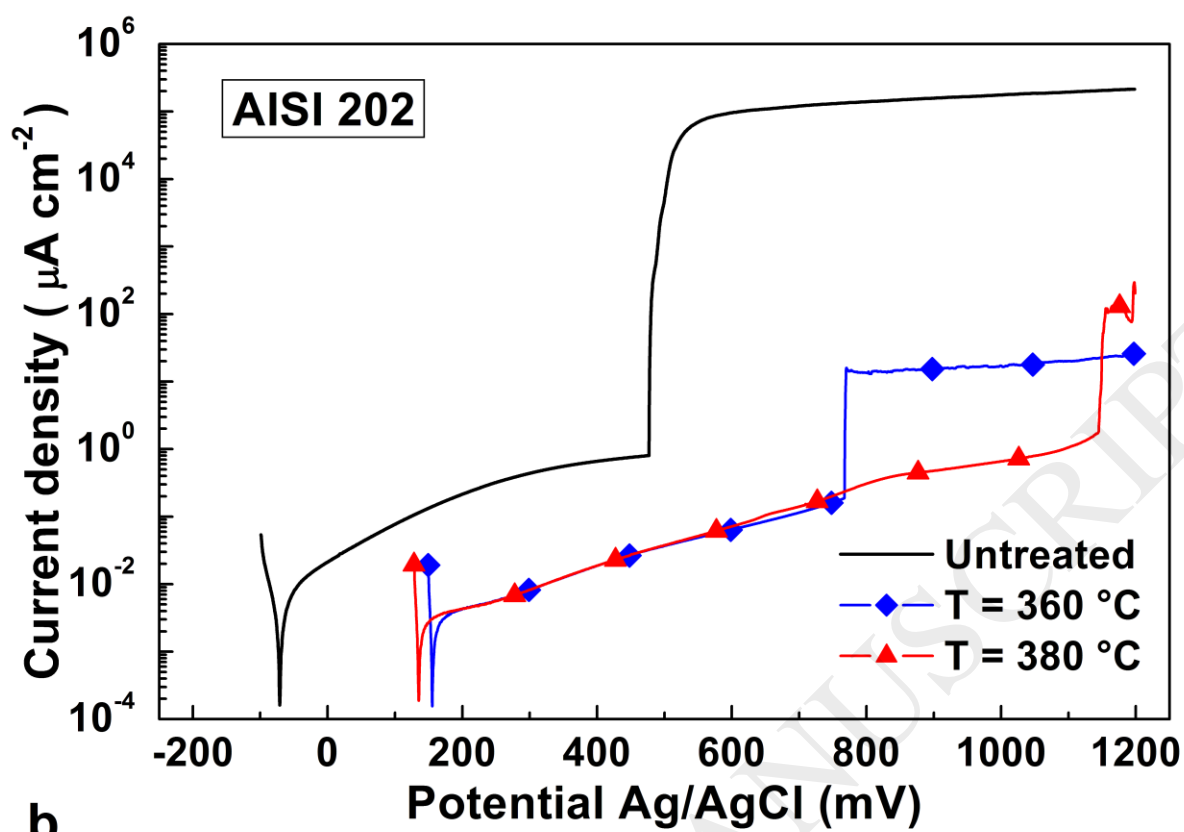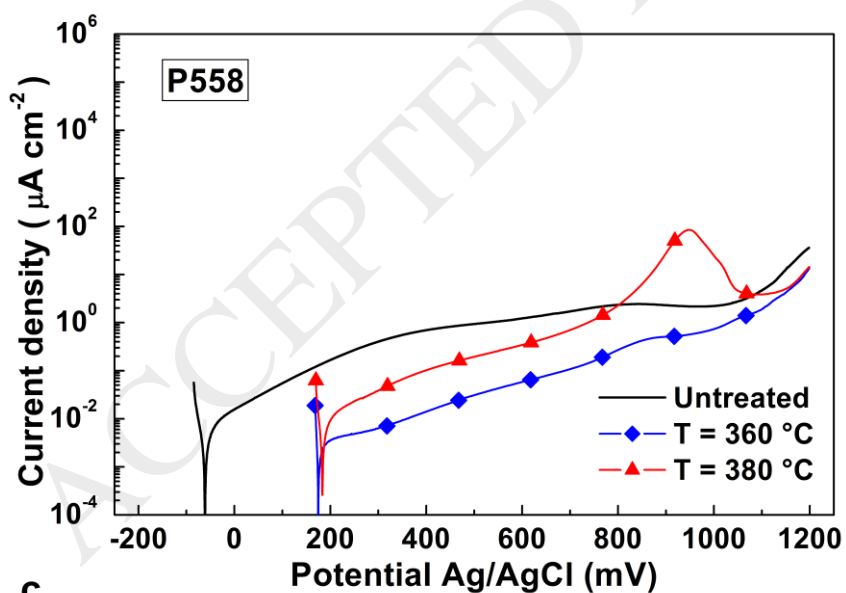
Fig. 11. Polarization curves of AISI 316L (a), AISI 202 (b) and P558 (c) samples untreated and

nitrided at the indicated temperatures (solution: 5 % NaCl, aerated).

Fig. 12. Surface morphology after potentiodynamic tests. Untreated samples: AISI 316L (a), AISI 202 (b), P558 (c). 360-°C nitrided samples: AISI 316L (d), AISI 202 (e), P558 (f). 380-°C nitrided samples: AISI 316L (g), AISI 202 (h), P558 (i). (Solution: 5 % NaCl, aerated).
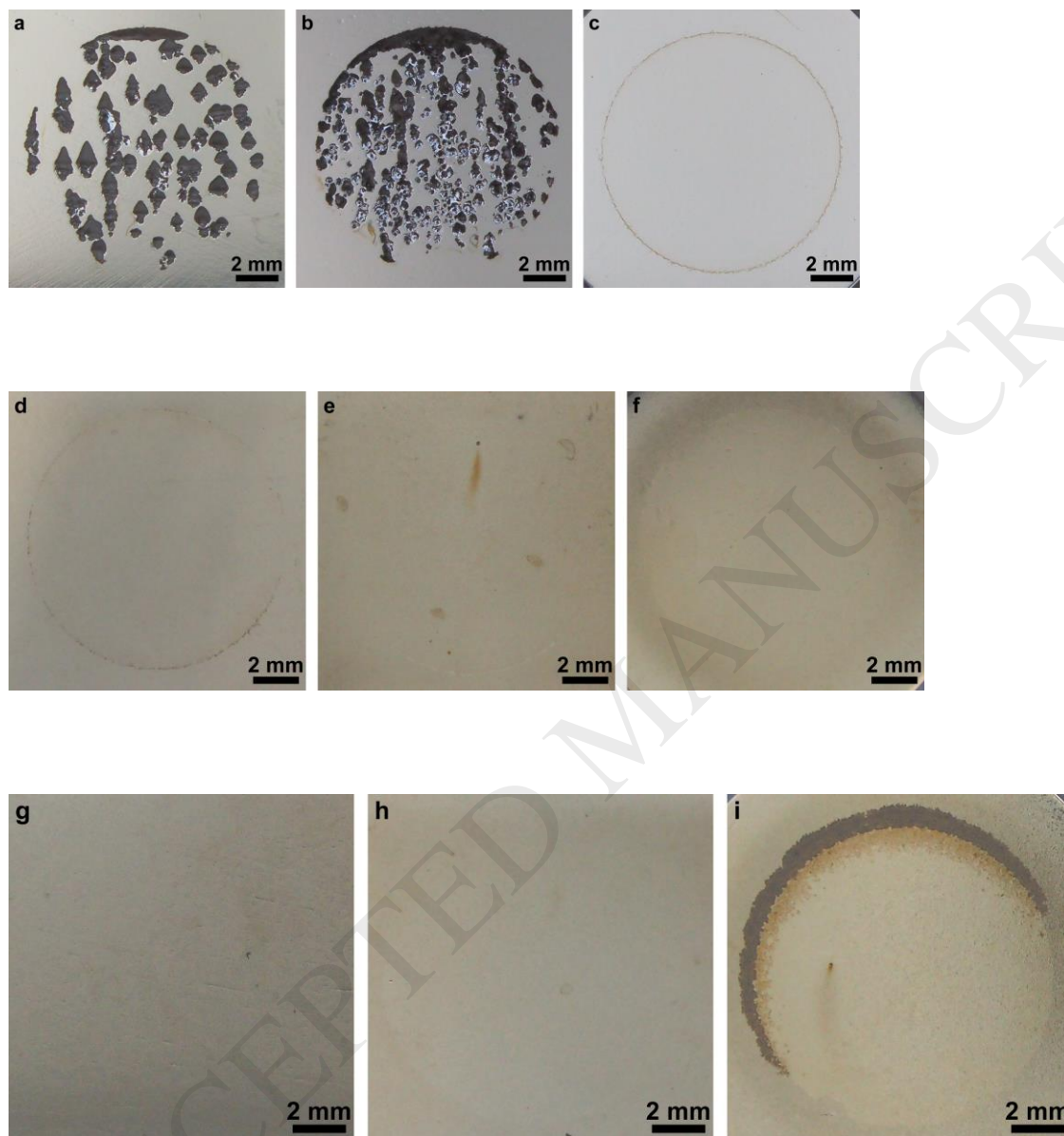

42

Fig. 13. Micrographs of the surface after potentiodynamic tests. AISI 316L samples nitrided at 360 (a) and 380 (b) °C; P558 samples nitrided at 360 (c) and 380 (d) °C. (Solution: 5 % NaCl, aerated).
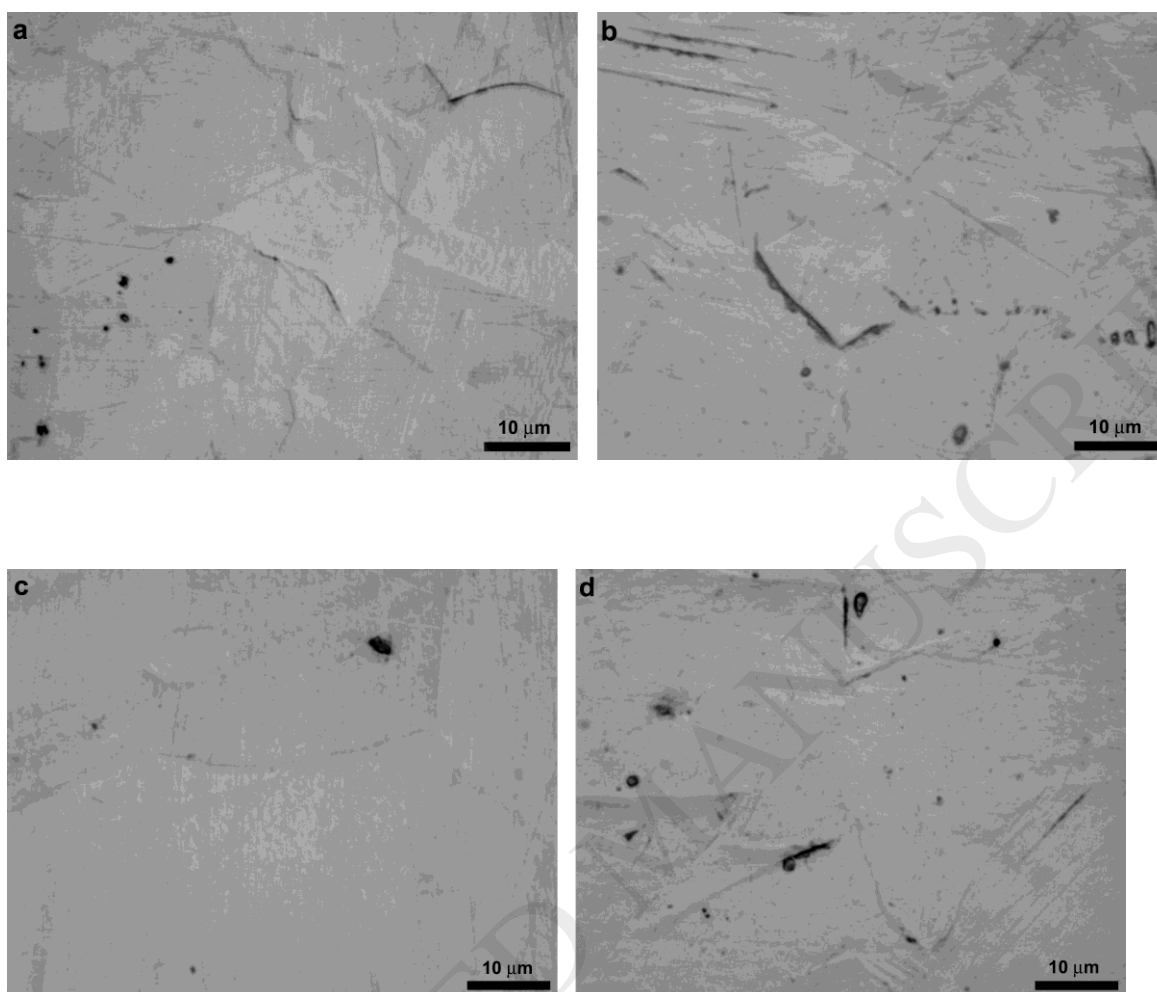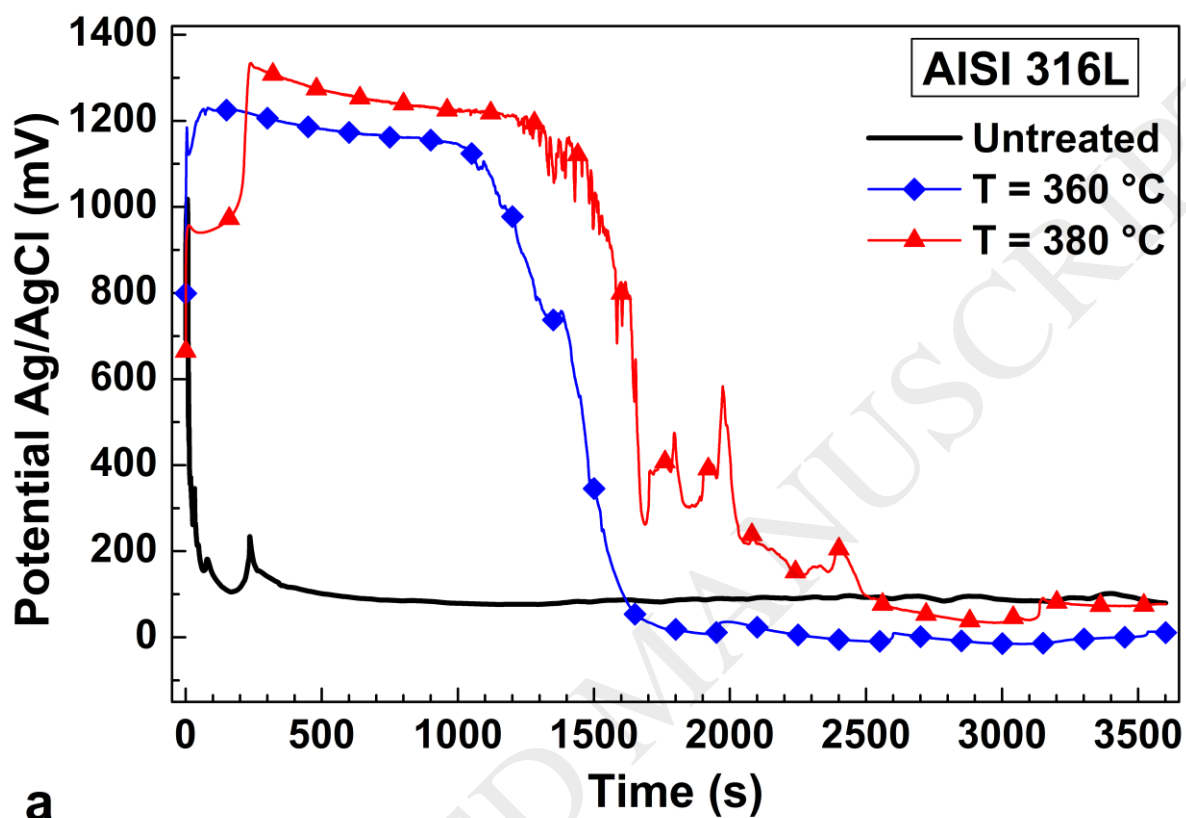
Fig. 14. Chronopotentiometric curves of AISI 316L (a), AISI 202 (b) and P558 (c) samples untreated and nitrided at the indicated temperatures (applied anodic current: 100 μA cm^{-2}; solution: 5 % NaCl, aerated).

a
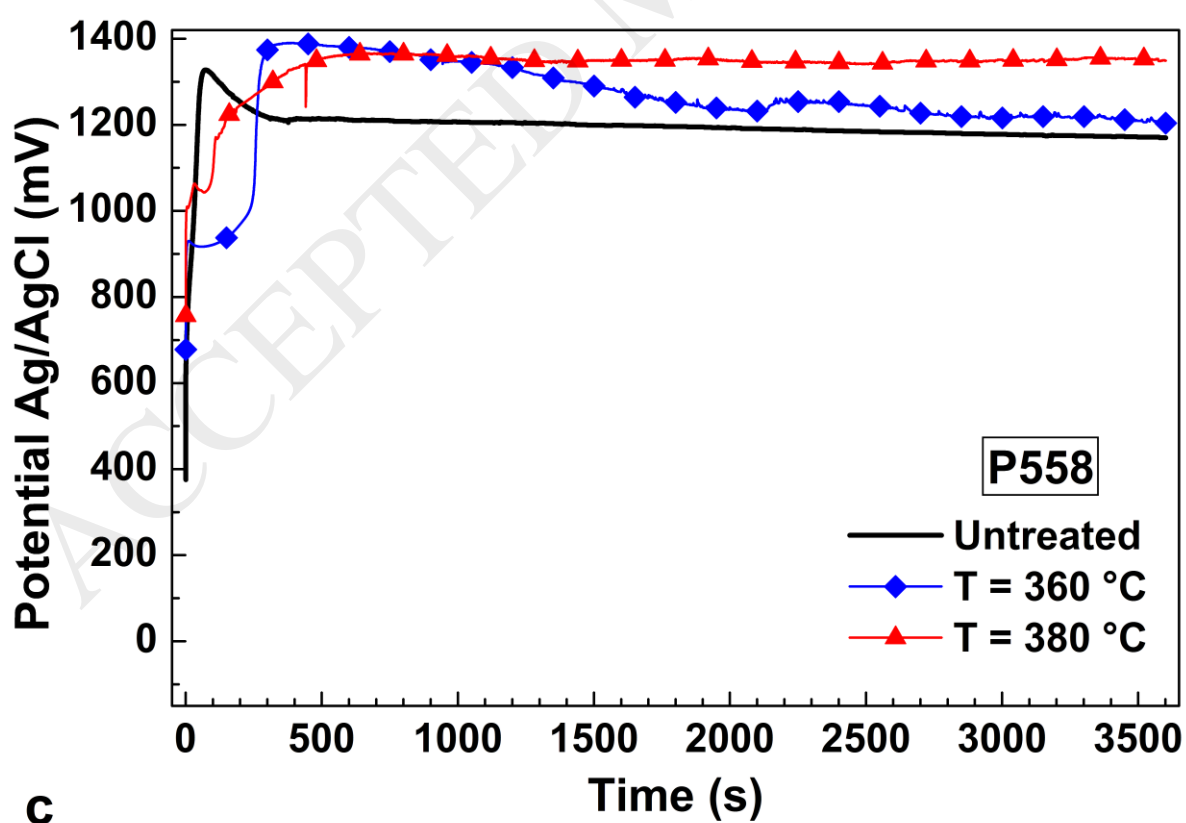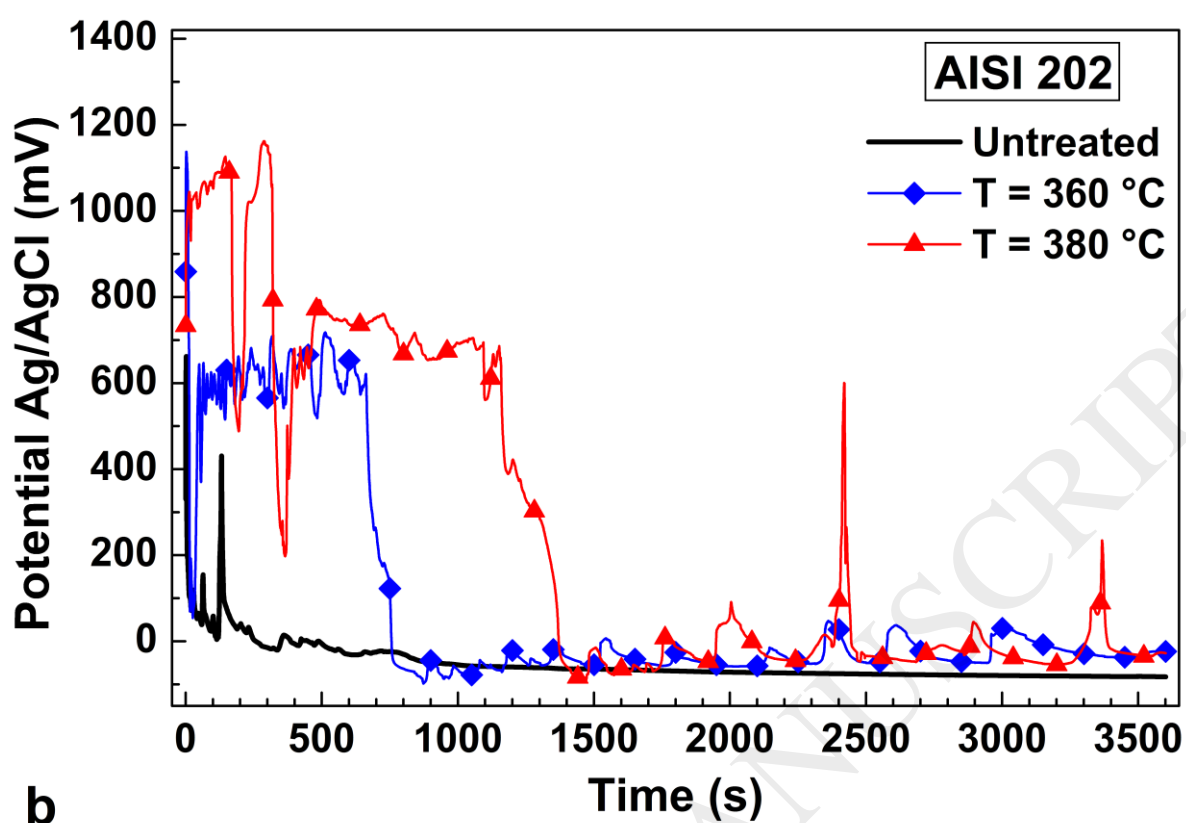
Fig. 15. Surface morphology after galvanostatic tests. Untreated samples: AISI 316L (a), AISI 202 (b), P558 (c). 360-°C nitrided samples: AISI 316L (d), AISI 202 (e), P558 (f). 380-°C nitrided samples: AISI 316L (g), AISI 202 (h), P558 (i). (Applied anodic current: 100 μA cm^{-2}; solution: 5 % NaCl, aerated).
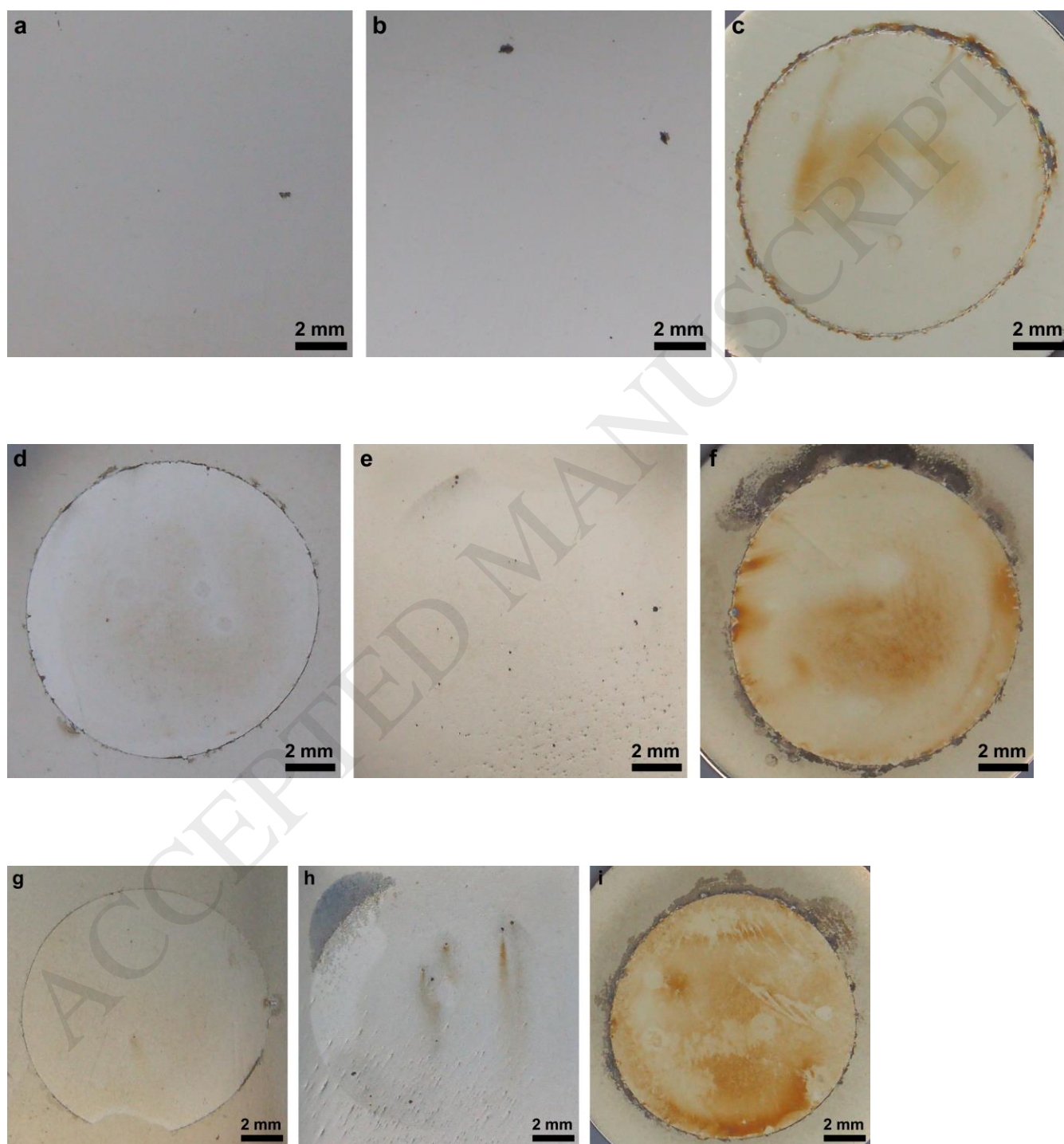
Fig. 16. Micrographs of the surface after galvanostatic tests. AISI 316L (a) and P558 (b) samples nitrided at 360 °C. (Applied anodic current: 100 μA cm^{-2}; solution: 5 % NaCl, aerated).
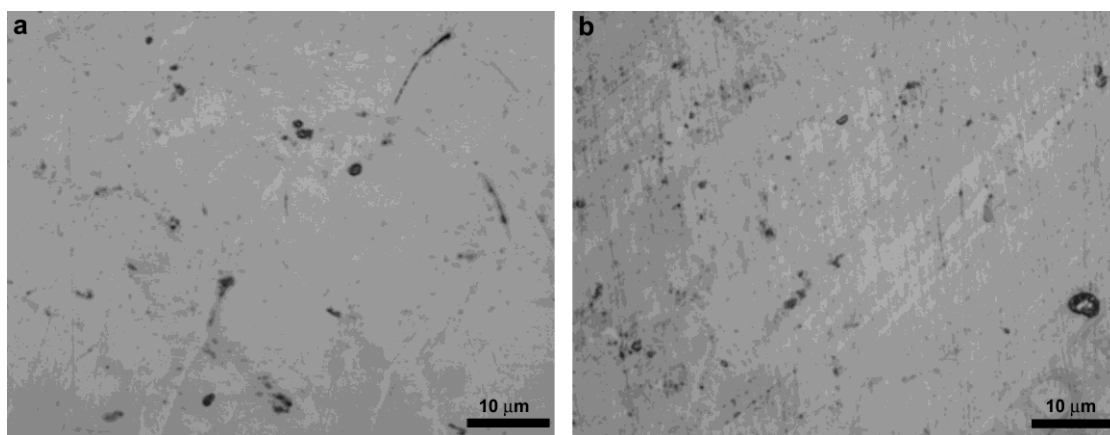
Table 1. Chemical composition (wt.%) of the used austenitic stainless steels

Material	Composition							
	C	Si	Mn	Cr	Ni	Mo	N	Fe
AISI 316L	0.029	0.34	0.9	16.6	10.3	2.01	0.049	Bal.
AISI 202	0.065	0.40	7.7	17.0	4.1	-	0.15	Bal.
P558	0.20	0.45	10.5	17.7	0.05	3.0	0.53	Bal.

Table 2. Roughness parameters Ra, Rz and Rc for AISI 316L, AISI 202 and P558 samples untreated and nitrided as indicated

Sample type	Ra (μm)	Rz (μm)	Rc (μm)
AISI 316L - untreated	0.005 ± 0.001	0.036 ± 0.003	0.022 ± 0.001
AISI 316L - nitrided 360 °C	0.030 ± 0.005	0.27 ± 0.04	0.18 ± 0.04
AISI 316L - nitrided 380 °C	0.057 ± 0.006	0.45 ± 0.06	0.27 ± 0.04
AISI 202 - untreated	0.006 ± 0.001	0.042 ± 0.008	0.027 ± 0.007
AISI 202 - nitrided 360 °C	0.023 ± 0.003	0.21 ± 0.03	0.14 ± 0.04
AISI 202 - nitrided 380 °C	0.055 ± 0.005	0.43 ± 0.04	0.27 ± 0.03
P558 - untreated	0.006 ± 0.001	0.040 ± 0.006	0.025 ± 0.004
P558 - nitrided 360 °C	0.017 ± 0.003	0.14 ± 0.03	0.09 ± 0.02
P558 - nitrided 380 °C	0.041 ± 0.003	0.32 ± 0.04	0.22 ± 0.03

Table 3. Thickness of the outer (d_o) and inner (d_i) modified layers of AISI 316L, AISI 202 and P558 samples nitrided at different temperatures (T)

Steel type	T (°C)	d_o (μm)	d_i (μm)
AISI 316L	360	1.5 ± 0.1	1.2 ± 0.1
AISI 202	360	1.5 ± 0.1	1.3 ± 0.2
P558	360	1.4 ± 0.2	1.6 ± 0.2
AISI 316L	380	3.7 ± 0.3	2.0 ± 0.2
AISI 202	380	3.8 ± 0.3	2.4 ± 0.2
P558	380	3.4 ± 0.2	3.0 ± 0.2

Table 4. Best fitting EEC parameter values for EIS spectra of untreated and nitrided AISI 316L, AISI 202 and P558 samples tested in aerated 5 % NaCl at the respective OCP (model: see Fig. 10 a)

Sample type	R_s (Ω cm^2)	R_{ct} (MΩ cm^2)	CPE$_{dl}$ x 10^5 (Ω^{-1} s^n cm^{-2})	n_{dl}	R_o (MΩ cm^2)	CPE$_o$ x 10^5 (Ω^{-1} s^n cm^{-2})	n_o	R_{tot} (MΩ cm^2)
AISI 316L – untreated	5.8 ± 0.2	0.8 ± 0.1	2.6 ± 0.3	0.94 ± 0.1	2.3 ± 0.4	1.0 ± 0.2	0.95 ± 0.04	3.1 ± 0.5
AISI 316L – nitr. 360 °C	5.2 ± 0.1	1.5 ± 0.1	1.6 ± 0.1	0.94 ± 0.01	32 ± 7	0.21 ± 0.01	0.97 ± 0.2	34 ± 7
AISI 316L – nitr. 380 °C	5.1 ± 0.1	0.8 ± 0.2	1.6 ± 0.1	0.96 ± 0.01	242 ± 80	0.25 ± 0.03	0.83 ± 0.05	243 ± 80
AISI 202 – untreated	5.4 ± 0.2	0.8 ± 0.1	3.2 ± 0.1	0.95 ± 0.01	1.4 ± 0.3	1.4 ± 0.2	0.93 ± 0.07	2.2 ± 0.4
AISI 202 – nitr. 360 °C	4.9 ± 0.2	1.2 ± 0.3	1.4 ± 0.3	0.91 ± 0.03	39 ± 8	0.9 ± 0.2	0.91 ± 0.03	40 ± 8
AISI 202 – nitr. 380 °C	5.2 ± 0.1	0.8 ± 0.2	1.6 ± 0.1	0.96 ± 0.01	323 ± 80	0.26 ± 0.01	0.82 ± 0.03	324 ± 80
P558 – untreated	5.6 ± 0.1	1.0 ± 0.2	3.1 ± 0.1	0.94 ± 0.01	2.9 ± 0.5	0.82 ± 0.06	0.91 ± 0.03	3.9 ± 0.7
P558 – nitr. 360 °C	5.1 ± 0.1	0.8 ± 0.3	2.1 ± 0.2	0.95 ± 0.01	154 ± 60	0.47 ± 0.09	0.88 ± 0.03	155 ± 60

Table 5. Best fitting EEC parameter values for EIS spectra of 380°-C nitrided P558 samples tested in aerated 5 % NaCl at the respective OCP (model: see Fig. 10 b)

R_s (Ω cm^2)	R_1 (kΩ cm^2)	CPE$_1$ x 10^5 (Ω^{-1} s^n cm^{-2})	n_1	R_2 (MΩ cm^2)	CPE$_2$ x 10^5 (Ω^{-1} s^n cm^{-2})	n_2	R_3 (MΩ cm^2)	CPE$_3$ x 10^5 (Ω^{-1} s^n cm^{-2})	n_3	R_{tot} (MΩ cm^2)
5.5 ± 0.2	1.6 ± 0.3	2.5 ± 0.3	0.92 ± 0.02	1.9 ± 0.3	0.8 ± 0.2	0.87 ± 0.03	261 ± 80	0.7 ± 0.2	0.82 ± 0.06	263 ± 80

Table 6. Average corrosion potential, E_{corr}, passive current, i_p, pitting potential, E_{pit} (evaluated as the potential beyond which the anodic current density last crossed 5 µA cm^{-2} before the end of the corrosion test), charge for unit surface of zone I (from E_c to +500 mV (Ag/AgCl)), Q_I, of zone II (from +500 to +1000 mV (Ag/AgCl)), Q_{II}, and of zone III (from +1000 to +1200 mV (Ag/AgCl)), Q_{III}, of AISI 316L, AISI 202 and P558 samples untreated or nitrided as indicated (solution: 5% NaCl, aerated).

Sample type	E_{corr} (mV (Ag/AgCl))	i_p (µA cm^{-2})	E_{pit} (mV (Ag/AgCl))	Q_I (mC cm^{-2})	Q_{II} (mC cm^{-2})	Q_{III} (mC cm^{-2})
AISI 316L – untreated	-59 ± 5	0.32 ± 0.04	$+570 \pm 40$	1.6 ± 0.5	$(1.0 \pm 0.2)\,10^5$	$(1.1 \pm 0.1)\,10^5$
AISI 316L – nitr. 360 °C	$+171 \pm 20$	0.20 ± 0.02	$+1142 \pm 5$	0.012 ± 0.001	0.46 ± 0.08	3.3 ± 0.5
AISI 316L – nitr. 380 °C	$+174 \pm 10$	0.22 ± 0.01	$+1194 \pm 10$	0.013 ± 0.001	0.50 ± 0.09	1.1 ± 0.3
AISI 202 – untreated	-71 ± 5	0.29 ± 0.01	$+470 \pm 10$	220 ± 40	$(1.9 \pm 0.2)\,10^5$	$(1.2 \pm 0.1)\,10^5$
AISI 202 – nitr. 360 °C	$+135 \pm 20$	0.03 ± 0.01	$+710 \pm 30$	0.017 ± 0.003	11.5 ± 0.5	27 ± 2
AISI 202 – nitr. 380 °C	$+174 \pm 15$	0.13 ± 0.04	$+1123 \pm 30$	0.012 ± 0.002	0.30 ± 0.09	12 ± 3
P558 – untreated	-70 ± 10	0.34 ± 0.01	$+1103 \pm 5$	0.65 ± 0.08	1.9 ± 0.1	6.4 ± 0.6
P558 – nitr. 360 °C	$+152 \pm 20$	0.22 ± 0.04	$+1147 \pm 15$	0.013 ± 0.001	0.39 ± 0.05	2.1 ± 0.2
P558 – nitr. 380 °C	$+170 \pm 20$	0.23 ± 0.01	$+1129 \pm 20$	0.062 ± 0.016	6.9 ± 0.6	5.2 ± 0.5

Table 7. Average maximum (E_{maxI}, E_{maxII}) and minimum (stationary) (E_{minI}, E_{minII}) potential values recorded for untreated and nitrided AISI 316L, AISI 202 and P558 samples tested galvanostatically in aerated 5 % NaCl (applied anodic current: 100 μA cm^{-2}).

Sample type	E_{maxI} (mV (Ag/AgCl))	E_{maxII} (mV (Ag/AgCl))	E_{minI} (mV (Ag/AgCl))	E_{minII} (mV (Ag/AgCl))
AISI 316L – untreated	+955 ± 45	−	+80 ± 10	−
AISI 316L – nitr. 360 °C	+1205 ± 18	+1240 ± 10	+1147 ± 10	+11 ± 10
AISI 316L – nitr. 380 °C	+960 ± 20	+1334 ± 10	+1210 ± 15	+70 ± 20
AISI 202 – untreated	+640 ± 40	−	-83 ± 5	−
AISI 202 – nitr. 360 °C	+1075 ± 60	+850 ± 80	+580 ± 50	-24 ± 20
AISI 202 – nitr. 380 °C	+1150 ± 80	+1082 ± 80	+680 ± 30	-28 ± 20
P558 – untreated	+1328 ± 15	−	+1170 ± 10	−
P558 – nitr. 360 °C	+950 ± 20	+1392 ± 10	+1330 ± 20	+1204 ± 20
P558 – nitr. 380 °C	+1063 ± 20	+1366 ± 10	+1350 ± 10	−